CHAPTER 2
PHYSICAL METALLURGY OF SOLDER-SUBSTRATE REACTIONS

A. D. Romig, Jr., Y. A. Chang, J. J. Stephens,
D. R. Frear, V. Marcotte and C. Lea

Introduction

The physical metallurgy of solder joints is of great interest both from a fundamental scientific perspective and because of its technological importance. The reliability of the joint is associated with the wettability of the surfaces to be joined and the joint's subsequent ability to retain performance integrity. Understanding the reactions that occur during soldering and subsequent aging must ultimately come from a fundamental knowledge of the thermodynamics and kinetics of the solder–substrate system.

An understanding of solder–substrate reactions is needed to evaluate solder joint reliability. If a molten solder does not wet a substrate, the joint will not form and result in poor reliability. In most cases, the formation of an intermetallic compound, by the reaction of the solder with the substrate, occurs during the wetting process. However, excessive exposure of the substrate to the molten solder may produce compositions that actually cause the solder to de-wet. The manner by which a solder joint ages is also important with respect to reliability. If the intermetallic phases that form are excessively brittle, the joint may not be able to withstand normal operating strains. If the intermetallic layer grows too quickly, the solder joint may become depleted of the elemental constituent used to form the intermetallics and thereby change the properties of the joint. The interdiffusion processes which produce the intermetallic layer can also produce Kirkendall porosity which also can degrade the mechanical properties of the joint. The examples discussed in this chapter show that the solder–substrate reaction can be critical to solder joint behavior.

The thermodynamics of the molten solder–substrate reaction determine whether the solder will wet the surface. With sufficient information it is possible to model the reaction and therefore predict the solderability of the system. A thermodynamic and kinetic understanding can also be used to study and model which phases (intermetallics) will form at the solder–substrate interface during the soldering reaction. If the data are available for a specific system, the kinetics of the intermetallic compound formation during wetting can also be modeled.

The solid-state reactions between the solder and substrate can also be described given sufficient thermodynamic and kinetic data. However, such data are often only available for simple two-component systems. Typical solder joints are at least ternary systems thereby increasing the complexity of the analysis. Due to the complex nature of the fundamental thermokinetic analyses and the lack of thermokinetic data, many of the published models are empirical. This chapter discusses the basic fundamentals of solder–substrate reactions, phenomenological thermokinetic modeling methods, and a survey of published empirical results.

The chapter is organized in a loosely chronological manner, *vis a vis* the formation and subsequent lifetime of a solder joint. The first reaction to occur is the wetting of the substrate by the molten solder. The thermodynamics of the

Solder Mechanics - A State of the Art Assessment
Edited by Darrel R. Frear, Wendell B. Jones
and Kenneth R. Kinsman
The Minerals, Metals & Materials Society, 1991

wetting reaction are discussed along with the experimental methods used to measure wetting. Intermetallic compounds nucleate and grow during the wetting process and in the solid state during the subsequent processing, storage and service lifetime of the joint. A survey of the literature is included which discusses intermetallic formation and growth. Formalisms to model and predict intermetallic formation and growth based on a more fundamental phenomenological methodology are also discussed. These models, based on phase diagram and kinetic information, are presented and their utility examined through the use of case examples.

Solderability - Wetting Phenomena

INTRODUCTION TO SOLDERABILITY

Solderability is a property of electronic and other components that is crucial both to the efficiency of manufacture and to the reliability of the product. Solderability is important for three basic reasons:

- Good component solderability allows the use of less active fluxes, thereby reducing the requirement for cleansing flux residues. This is an environmental benefit. The removal of flux residue has the additional benefit of eliminating potential corrosion problems due to that residue.

- Good component solderability produces greater "first pass" soldering yields and consequently less hand reworking of the solder joints. This is important since reworking may reduce the fatigue performance of a joint compared with a successful first-pass joint.

- Good component solderability results in a greater uniformity of solder fillet, with a geometry that is close to the ideal for maximum fatigue performance.

Solderability is dependent upon the wettability of the two surfaces being joined. Poor component solderability can, to some extent, be overcome by the use of more active fluxes, but the trend towards denser component packing leads to difficulties in removing flux residue after assembly. Therefore, less active fluxes are preferred. Environmental concerns are also becoming more important. The problems of inspection, testing, and component replacement or solder fillet rework increase the desirability defect-free soldering. Solderability is therefore an increasingly important manufacturing issue.

The solderability of a component, defined as the suitability of the component to be soldered by a given method, is a complex processing parameter. A major unresolved gap in the understanding of the soldering process is the relationship between wettability and solderability. As described later, wettability can be directly measured. Solderability can not be directly measured in a quantifiable way and its relationship to wettability has not yet been explicitly defined.

There are three important aspects to solderability: thermal demand, wettability, and resistance to soldering heat. The thermal characteristics of the component must allow the joint to be heated to the soldering temperature within the

specified time. The solderable surfaces must allow the molten solder to wet and spread during the available time without subsequent de-wetting. The soldering heat and the induced thermal stresses associated with it must not affect the functioning of the components. Each of these three aspects of solderability can be engineered to fit the particular application by a suitable choice of component materials and attention to process control. The most restraining of the three parameters in regard to design for performance is the component wettability.

Solderability is too broad a topic to be covered in a few pages and therefore only an overview is given here. The emphasis here is on the engineering, rather than fundamental physics, aspects of wettability and solderability. Readers are referred to other sources for a more in-depth analysis [1–4].

WETTABILITY

When discussing the wetting characteristics of a surface by molten solder, there are two important factors: 1) the extent of wetting and 2) the rate of wetting [5]. The degree of wetting (as indicated by the contact angle) is an equilibrium case governed by the laws of thermodynamics and dependent on the surface and interfacial energies involved at the liquid - solid interface. The rate of wetting (how fast the solder wets and spreads) is governed by the thermal demand of the system, the ability of the heat source to supply heat, the efficacy of the flux, the viscosity of the solder and the chemical reactions occurring at the interfaces.

Physics of Wetting

The physics of wetting is governed by Young's Equation (In 1805, Young described the problem qualitatively and Depre put it in mathematical terms in 1869). The system strives towards a minimum total free energy. The Young (Young–Dupre) Equation follows:

$$\gamma_{SV} = \gamma_{SL} + \gamma_{LV}\cos\theta \qquad (1)$$

where the subscripts γ_{SV}, γ_{SL}, and γ_{LV} refer to the solid-vapor, solid-liquid, and liquid-vapor surface tensions, respectively. For soldering, the vapor phase will be replaced in nearly all processes by flux.

For optimum wetting, the contact angle, θ, must be minimized and therefore γ_{SV} must be maximized. Oxides and contamination lower the surface energy of the substrate. The most important function of the flux is to remove or disperse oxides and contaminants and thereby increase γ_{SV}. During soldering, the flux also maintains a local environment around the surfaces being joined which protects them from re-oxidation as well as enhancing heat transfer from the heating source to the substrate and solder.

Equation 1 shows that wetting is also enhanced by minimizing γ_{LV}. This value is commonly referred to as the surface tension of solder. Although γ_{LV} is a function of the solder composition, the flux covering the liquid solder, and the temperature, it is normally close to 0.4 J/m.

The wetting phenomenon is simplistically described by Young's equation; the wetting angle is determined only by a balance of surface tension terms. If there is no chemical reaction between the liquid and the solid substrate and the substrate is perfectly smooth, Young's equation as given in Equation 1 is correct. However, in the case of a solder wetting a metallic substrate a chemical reaction forming one or more intermetallic compounds, will occur. This reaction alters the surface energies which influences wetting. The free energy contribution to wetting has recently been described [6]. In many systems, the free energy change due to the chemical reaction actually dominates that due to surface tension forces. The predictions of this thermodynamic analysis are borne out by experimental observations, but a systematic study has yet to be done.

The formation of intermetallic compounds may influence Young's equation in yet another way. These intermetallic compounds influence the value of γ_{SL}, and hence influence both the degree and rate of wetting. The influence of this term has been recognized [6], but the magnitude has not yet been calculated quantitatively.

Materials Used in Soldering

The substrate and solder materials used in electronics assembly are chosen considering the requirements of design and manufacturability. Important manufacturability issues include solderability and the thermal characteristics of the materials being joined.

Substrate Materials

Wettable materials such as Cu and Ni and their alloys are common substrate materials. When clean, these surfaces are readily wet by solder using mild fluxes, but become increasingly difficult to wet as they oxidize. Quite often a thin Au layer is plated on the surface to alleviate this problem and retain wettability during storage.

Other component types, notably ceramic chip capacitors, are fabricated using a fired conductive AgPd ink as the solderable metallization. The solderability of these surfaces is often poor, more as a result of their roughness and porosity than intrinsically poor wettability. The solderability of such surfaces degrades only very slowly during storage unless the air is contaminated with H_2S or SO_2 which causes the Ag to undergo sulfidation. For more high-reliability applications, Au and Pt–Au thick films are often used. These films are more inert than Ag films but are, of course, more expensive.

The solderability of metals and conductive inks is enhanced by using a fusible solderable coating (a layer is molten at the soldering temperature). The coating is usually Sn, SnPb, or PbIn and is applied either by plating or dipping.

Solders

The most common solders used in the electronics industry are based on combinations of Pb and Sn, and the near eutectic 60–62 wt.% Sn, balance Pb is the most prevalent. For manufacturing situations where a sequence of solder operations are required, each at a successively higher temperature, higher Pb

containing solders can be used. Occasionally In–Pb solders are also used, especially if the surfaces to be joined are metallized or coated with Au. In this case, the Pb–In solder is preferred because it has a lower solubility for Au than the Sn–Pb solder. For lower melting alloys, Bi, Cd, In and Sb are added to the Pb–Sn alloys. For more information on the metallurgy of solders, see Chapter 1.

Fluxes

Fluxes are used primarily to improve the wetting properties of the solder - substrate system. Flux increases the surface tension, γ_{SV}, of the substrate by removing oxides and other surface residues. It also prevents oxidation of both the solder and substrate and can have an influence on reducing the vapor-liquid surface energy. As a result, wettability is enhanced.

In the electronics industry, the most common fluxes are rosin based. There are three classes of rosin-based fluxes defined according to their activity:

- RA–Activated fluxes containing a strong ionic activator, normally a halide
- RMA–Mildly activated fluxes with lower concentrations of halides or activated with organic acids (halide free)
- R–Rosin without any activators added, depending upon the very weak organic acids in natural rosin for the fluxing action.

Water soluble fluxes are being studied extensively because of restrictions on carcinogens and chlorinated fluorocarbons (CFCs) typically used for cleaning. There remains, however, the problem of water effluent containing Pb- and Sn-bearing flux residues.

Fluxes by their nature must be acidic to dissolve or fragment metal oxides. A potential disadvantage of the fluxing action is the possibility of redeposition of metal solutes on other parts of the circuit. For example, In (and to a lesser extent Sn) are soluble in rosin-based fluxes [8], and solute redeposition can lead to the loss of surface resistivity of a circuit.

A recent article [9] has shown that organic fluxes contain organic, metallic oxide and inorganic particulate. Some of the inorganics are sulfides. No problems have been attributed to these particles but a more systematic investigation is needed.

For the reasons cited above, there has been a trend to minimize the use of highly active fluxes. Rather the use of less active fluxes and water soluble fluxes is becoming more common. Fluxless joining is also being investigated. The fluxless approach ranges from property additives to solder paste (which leave no residue) to the use of reactive gases, plasmas, lasers (all of which may be difficult to incorporate into manufacturing processes) and mechanical activation (e.g., ultrasonics).

MEASUREMENT OF WETTING

Engineers have attempted to evaluate soldering using controlled testing methods designed to replicate the actual soldering process. A key aspect of this testing is the direct measurement of wettability. The experimental test methods for determining the wettability range from the simple dip tests to the recent and quantifiable wetting balance. In all cases, the use of these methods has been driven by a desire to improve the control of wetting and bonding of components. The main criterion for wetting test selection is the desire to replicate the manufacturing process by the wetting test. This is not always possible and leads to certain compromises in the testing method.

Degrees of Wetting

Unfortunately, not all processes lead to the desired result of complete wetting. There are various defined degrees of wetting: fully wet, nonwet, partially wet and dewet. The assignment of a wetting descriptor is primarily based on the visual appearance of the wetted surface. The assignment of a degree of wetting is somewhat qualitative and is usually defined by the value of the contact angle, θ.

Fully Wet

This is the optimum condition where complete wetting has occurred and a metallurgical bond has formed. The contact angle for the fully wet condition is $\theta \sim 0$.

Nonwet

Non-wetting is the condition in which a metallurgical bond has not formed. The contact angle for the nonwet condition is $\theta > 90$ degrees.

Partially Wet

Partial wetting is defined as the case in which a metallurgical bond has formed, but the contact angle is larger than zero. Partial wetting is defined solely on the basis of visual observation. The contact angle for partial wetting is $0^\circ < \theta \leq 90^\circ$.

De-Wetting

In this case, the substrate appears to initially wet fully. After a period of time, however, the molten solder begins to recede (ball-up), exposing substrate area which had initially been covered by molten solder. Dewetting is usually caused by extensive growth of an intermetallic or after the solder–substrate reaction has reached an impurity inclusion.

Techniques to Measure Wetting

Parallel Plates

This technique involves measuring the meniscus rise of the solder between two parallel plates. There is often very poor correlation between this test and actual production solderability.

Sessile Drop

In this test, a piece of solder of constant volume is placed on a substrate with a known flux volume at a temperature above the solder liquidus and held for a given period of time. This technique usually measures equilibrium wetting of the solder. One can measure the area of spread, the contact angle or the solder height [10]. The solder height method is fast, but it is somewhat inaccurate due to solidification shrinkage of the solder which is less than the height of the original liquid drop. The area of spread, contact angle, and solder height are geometrically interrelated for axi-symmetric drops and one can calculate any one parameter from the other two.

Dip Test

In this test, the component is prefluxed and heated prior to dipping into a solder bath that is held at a constant temperature. The piece is immersed at a known rate and held for a set time and then withdrawn at a known rate. The assessment of wettability is simply made from a visual judgement of the amount of solder which actually adhered to the metal surface.

Wetting Balance

One of the most recently developed test methods, the wetting balance, is extremely versatile and can address many of the criticisms of the wettability techniques (such as the need for an accurate quantitative measure of wetting properties) discussed above. One of the main advantages of the wetting balance technique is the ability to monitor and record explicitly wetting force as a function of time. The test is somewhat complicated, however, by the fact that the buoyancy force must be corrected for the density of the solder used in a specific experiment. The density correction is required to quantitatively compare wettability results for two different solders.

In the wetting balance test method, the specimen is suspended from a sensitive balance and immersed at a controlled rate (and to a set depth) into a bath of molten solder held at a desired temperature [11–13]. The specimen is subjected to time-variant, opposing vertical forces of buoyancy and surface tension which are detected by a transducer and converted to an electrical signal that is continually recorded on a computer [14–15].

This apparatus is a versatile wettability test because it can be used to assess the wettability of leaded insertion components, plate and wire substrates, as well as as evaluate the efficacy of fluxes. For use with surface mount components, some modifications may be required.

The specimen is first fluxed and hung on the balance over the solder bath for a predetermined time such that it is effectively preheated by convection from the solder. The specimen is then immersed, usually at a speed of 15 mm/s, to a predetermined depth and held in that position for a specified time (usually about 10 – 20 s), before withdrawal. The force experienced by the specimen as a function of time is recorded.

Figure 1 shows the six stages of the testing of the specimen that is readily wet by the solder. (Figure 2 shows some representative curves.) In each case, the full

horizontal line represents the force condition at the start of the test cycle and the dotted horizontal line represents the buoyancy level at which the wetting force is zero (the contact angle is 90°). The buoyancy of the specimen is simply the product of the immersed volume (measured from the mean liquid level, not from the meniscus level) and the density of the solder.

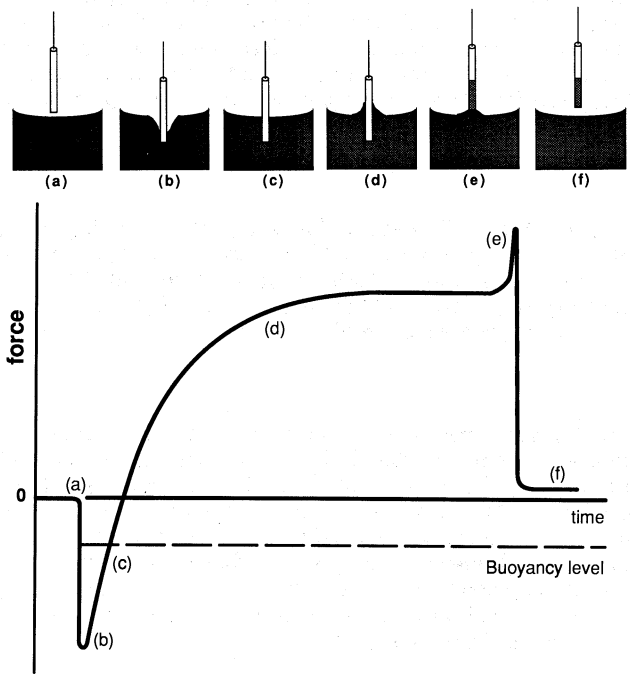

Figure 1 A wetting balance curve.

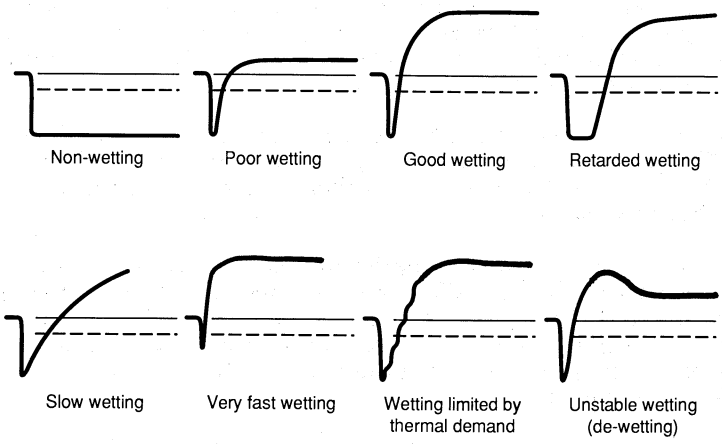

Figure 2 Some representative shapes of wetting balance curves.

For testing surface mount components, the solder bath can be replaced by a small molten globule of solder. This enables individual leads to be assessed sequentially. Furthermore, the solderable metallizations of leads on surface mount components are often smaller than the meniscus rise of solder. Hence, the wetting balance equilibrium force may well be constrained by a lack of substrate to wet. The use of a small globule overcomes this problem. The use of small solder volume is also more representative of solder paste reflow.

DETERIORATION OF WETTABILITY

An understanding of other factors that influence wetting is necessary to minimize those factors which limit solderability. When manufacturing engineers are faced with a wettability problem, a frequent solution is to use a more active flux rather than to investigate the source of the problem [16]. The root cause of the soldering difficulty, whether material or processing, is not often directly addressed. Due to many new concerns in industry, including reliability and cleaning, this *bandaid* approach will be used much less frequently in the future. Perhaps the most common cause of solderability difficulties is related to the loss of wettability as a component ages between assembly steps. The following paragraphs discuss the effects of aging on wettability and accelerated testing.

Mechanisms of Aging

There is often a considerable time interval between the initial fabrication of a component and and its use in a subsequent assembly step. Parts are stored under a variety of conditions, usually not controlled. Often, the wettability deteriorates during storage and in the extreme case, the part will not wet. Artificial accelerated aging tests can "predict" the effect of storage on wettability. Unfortunately, the correlation between accelerated and actual long-term aging is often poor. This occurs either because the artificial environments do not replicate the actual storage conditions, or because there are two or more mechanisms operating simultaneously to degrade the wettability. These mechanisms may have different activation energies such that one may predominate in accelerated aging, but another predominates during natural aging.

For nonfusible solderable surfaces such as Cu or Ni, wettability deteriorates as an oxide or corrosion film (such as a sulfide) develops on the surface. In general, a thicker oxide film requires a more active flux to disperse the oxide. Both the rate and the degree of wetting deteriorate during aging as the oxide grows. The problem is alleviated by one or all of the following:

- Storing in an inert atmosphere,
- Coating with a flash of Au, or
- Using a thick fusible coating of tin or solder.

Storage in an inert atmosphere eliminates oxygen or sulfur from contacting the substrate so that no oxides or sulfides form. The use of a Au film over a solderable surface prevents oxygen from contacting the surface. The Au itself does not extensively oxidize so its solderability does not degrade. However, if the Au plated film is too thin (< 1.3 μm), the film is porous and the gold does not act as an effective oxygen barrier. If the Au is too thick (> 3.2 μm) extensive intermetallics can form in the solder joint (this point is discussed in more depth

later in this chapter). The most common method to maintain solderability of electronic components is to place a fusible coating of Sn or SnPb, whether plated or hot dipped, on the surface of the component. Regardless of the actual coating alloy used, the coated part is said to have been *tinned*. For components which have been pre-dipped to preserve solderability, two mechanisms of wetting degradation occur during storage: (1) the formation of an oxide film on the outer surface and (2) the interdiffusion at the coating–substrate interface of the Sn and the Cu, Fe, or Ni in the substrate to form a layer of intermetallic compound. A fusible coating enhances wetting because the oxide film, formed on the coating rather than the substrate, will fragment and disperse more readily when the coating liquifies during the soldering process. The tinned coating must be sufficiently thick because during storage it continually thins due to the growth of nonfusible intermetallic compounds. Hence, both oxide film thickness and intermetallic compound thickness are important to wettability with respect to the thickness of the fusible coating.

The effects of surface oxidation and intermetallic growth can be seen from the variation of wetting time as a function of aging, as shown in Figure 3. During Stage 1, the wetting time increases due to increasing oxide thickness (e.g. which corresponds to an oxide film with decreasing porosity). During Stage 2, the oxide film may continue to thicken, but it is no more of an effective barrier to the molten solder than the oxide layer present in Stage 1. Hence, wetting time remains unchanged. After an extended period, the intermetallic compound layer begins to consume the fusible layer and may even begin to penetrate to the outer surface of the coating. Oxidized intermetallic compounds do not wet well. Therefore, the growth of intermetallic compounds to the extent that they reach the surface is responsible for Stage 3 deterioration.

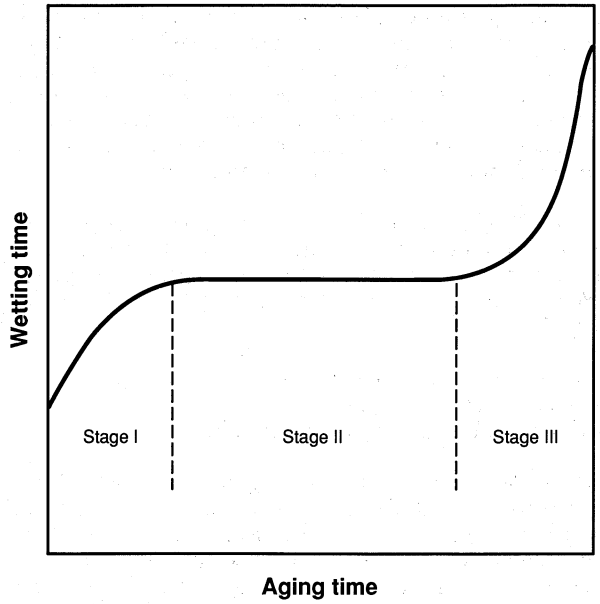

Figure 3 Schematic diagram of the wetting time of a solderable surface as it ages.

The aging time required to produce a given level of deterioration of wettability is a function of the fusible coating thickness as shown in the Figure 4. The curves are all similar to the one shown in Figure 3. For this particular system, a coating less than 2 μm thick will become unsolderable in a few months, but a coating of 8 μm should not deteriorate for several years.

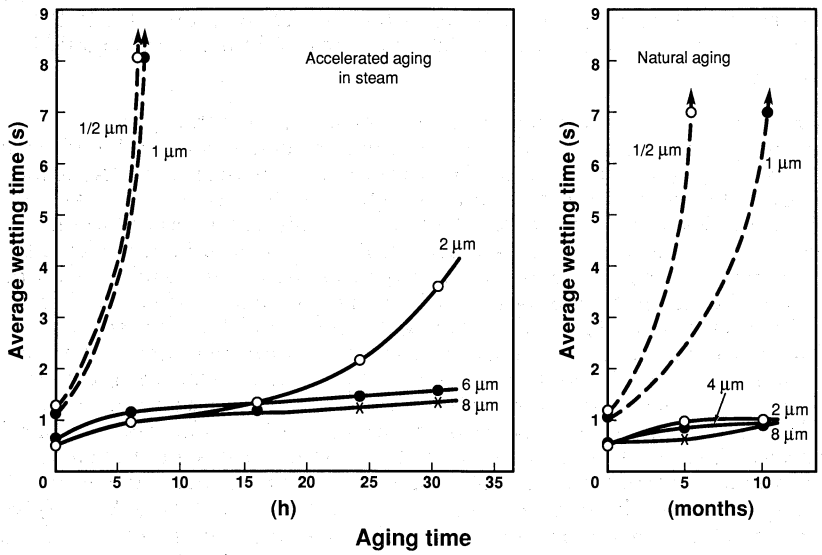

Figure 4 The wetting time for Sn-plated Cu wire as it ages naturally and in an accelerated steam-aging test, showing the effect of different coating thicknesses.

Wettability deterioration can be reduced by any or all of the following:

- Specifying a minimum tinned coating thickness of 5 μm.
- Storing the components in an inert atmosphere.
- Specifying a barrier layer beneath the fusible coating to reduce the rate of intermetallic compound growth (Ni–Sn compounds grow 20 times slower than Cu–Sn compounds and 120 times slower than Ag–Sn compounds at room temperature).

ACCELERATED AGING TESTS

An accelerated aging treatment is designed to reduce the solderability of a component at a rate that can be directly correlated to the reduction of solderability by natural aging. The lack of reliable data on the natural aging processes has led to the development of three different Accelerated Aging Tests:

- Dry heat, normally 155°C in air for 2, 16, 72, or 96 h.
- Damp heat, normally 40°C at 93% relative humidity for 4, 10, 21, or 56 days.
- Steam, with or without injected air, oxygen, SO_2, or other gases.

Disagreement over the validity of these tests has existed for years. Due to this uncertainty, many of the early accelerated tests may be in error and should be repeated [17].

One major criticism of accelerated aging treatments is that the aging mechanisms at the elevated temperature are not the same as those found during normal operating conditions. The dry heat procedure enhances both the oxide and intermetallic compound growth and therefore qualitatively replicates the two main processes of natural aging. The test is simple and it relates to all components except those with fired-on solderable inks that will not oxidize at 155°C. The damp heat procedure requires expensive equipment and is not widely used in manufacturing. Steam aging, without injected gas, is cheap and simple, but can give very misleading results. During the first 1 to 2 h of the test the wettability of the components actually can improve as contaminants are removed by the steam. Also, the degradation of wettability depends on the oxygen content of the steam and this is a strong function of the steam temperature near the component. The aging rate is maximized at around 95°C and decreases if the temperature is increased to 100°C. A better test is to inject gas into the steam to maintain a known partial pressure of oxygen. Even in this case, ambiguities exist. For example, a different result can arise if air, or a mixture of 80% N_2/20% O_2, is injected since the air contains a trace of CO_2 that produces an unsolderable lead carbonate on solder surfaces. To age solderable AgPd ink terminations in a controlled manner, traces of sulphur bearing gases can be used, either SO_2 or H_2S, using either the dry heat or steam tests.

CORRELATION OF WETTABILITY TESTING WITH ACTUAL PRACTICE–WETTABILITY TESTING AND MANUFACTURABILITY

One of the objectives of wettability testing is to assure high product yield. The testing methods discussed previously provide a part of that assurance. Furthermore, a functional test that relates wettability to actual solderability in manufacturing is needed. With the current level of understanding between solderability and wettability, actual component solderability is best monitored by statistical process control.

A case has been reported in which leads that exhibited significant de–wetting on wettability testing had visually acceptable fillets after assembly in wave soldering [18]. The source of the discrepancy was a consequence of the fact that the wettability test differed from the actual soldering process. In the actual assembly, solder can flow over dewetting defects and obscure them from external view. This is one example where the test predicted potential problems, but the parts passed visual inspection creating a potential in–service reliability problem. This example shows that one must be very careful in the design of tests,

their application to manufacturing processes, and the type of final inspection of the parts.

A case example [16] of product improvement using wettability tests involved a solderability problem where testing showed only 80% of the material would solder within 1.8 s. Statistically this correlated to 1 defective joint per 300 parts. A development team working with the supplier dramatically reduced the number of defective solder joints. Using the IEC Solder Globule Test and working to a general quality level for solder joints of 99.99% acceptance level, the soldering faults were reduced to a predicted one fault per one million joints. There was good correlation between the testing results and production. No faulty solder joints were found after 15 million production joints. The conclusion was that the globule test, supplemented with a de-wetting test, was required rather than a simple dip test [19].

SUMMARY OF WETTING AND SOLDERABILITY

Wettability is a strong function of substrate processing, purity of materials, pretinning type and thickness, solder composition, storage conditions and time, and reflow conditions. The variability observed in the product yield depends on these conditions. Therefore, for improved wetting, the effect of the above conditions must be understood and well controlled. To apply experimental test results to actual production, a correlation between testing and processing parameters must be established.

The future utility of wettability testing appears positive. Better instrumentation for the study of wetting is becoming available. In addition, cooperative studies to understand the relationship of wettability testing to manufacturability and field reliability are being conducted. There is a trend toward solving problems by improved processing rather than simply using a more active flux or changing the soldering time or temperature. Finally, the important task of establishing solderability standards and testing methods is underway.

Review of the Literature

EQUILIBRIUM SYSTEMS OF INTEREST TO SOLDERING TECHNOLOGY

Equilibrium phase diagrams can be used as a guide to identify which phases will be present as a result of either solder processing or long-term aging at specific temperatures. They are also useful in providing a ranking of substrate–solder interaction during soldering, since they can indicate the amount of solubility that a particular substrate metal has in a particular solder alloy. However, as is the case for most metallurgical systems, the equilibrium diagrams merely indicate what phases are thermodynamically stable, given a particular system composition and temperature; there may be other metastable phases that are not present on the equilibrium diagram that can form as a result of soldering. In addition, in systems (such as Pd–Sn) that exhibit numerous intermetallic phases, there is often no way to predict which of those equilibrium phases will actually be formed in a solder joint. In this sense, the solder–substrate interaction problem is as much a kinetics problem as it is a thermodynamics problem.

The work of Haimovich [20] provides an example of metastable phase formation in soldering systems. Aged Cu substrates with a 100 μinch (2.5 μm) overplate of Ni, along with either reflowed matte Sn or 90Sn–10Pb alloy (**Note:** all compositions given throughout this chapter are in weight percent, unless specifically stated otherwise), were observed to form platelets of the non-equilbrium phase $NiSn_3$ in addition to the equilibrium phase Ni_3Sn_4. The $NiSn_3$ phase is undesirable because it degrades the solderability of surfaces on which it is present. However, solderability could be restored by means of thermally decomposing $NiSn_3$, which produces Sn and the equilibrium phase Ni_3Sn_4. Using differential scanning calorimetry (DSC), Haimovich examined the kinetics of decomposition of $NiSn_3$. Isothermal DSC curves were analyzed using the Mehl-Johnson-Avrami equation, and the results indicated that the decomposition reaction occurs within 3 s at 250°C, while the decomposition reaction requires about 10^5 s at 215°C. Thus, higher temperature soldering processes for 60Sn–40Pb such as wave soldering (process temperature ~260°C) may not be impacted by the presence of $NiSn_3$, while lower temperature soldering processes such as vapor phase reflow (process temperature ~215°C) would require the removal of this phase prior to soldering.

Despite the previously discussed example involving metastable phases, it is useful to examine the various binary phase diagrams that may apply to common solder–substrate systems. A complete set of binary equilibrium diagrams is readily available [21], and should be consulted in order to obtain information concerning phase compositions. Recently, detailed thermodynamic assessments have been performed on a number of binary systems that are important for soldering technology, including the Au–Sn and Au–In systems [22, 23]. These assessments are useful because they often include thermodynamic quantities such as the free energy of formation for the various intermetallic compounds contained within a binary system.

The use of binary phase diagrams is especially effective when one of the major alloying elements in the solder is more reactive than the other. For example, Cu reacts with Sn but not with Pb; hence, the Cu–Sn binary system provides a reasonably complete description of which phases form for the case of Cu in contact with eutectic 63Sn–37Pb solder. However, there are many solder alloys that contain two or more reactive elements, and the solder–substrate reaction products that form are actually ternary intermetallics. One notable example is the case of the 50Sn–50In solder alloy in contact with Cu [24, 25]. For this particular system (Cu–Sn–In), there has been no systematic study of the appropriate ternary phase diagram, and thus it is difficult to predict what compounds would form without the benefit of extensive microanalytical characterization.

Fortunately, there have been a number of studies conducted on other ternary systems that are important to soldering technology. A brief survey of these studies [26–42] is presented in Table 1. Table 1 indicates that the majority of these studies have examined only isolated sections of these diagrams, although there are a number of examples (for example, the Au–Sn–Pb, Cu–Pb–Sn and Cu–Sb–Pb systems) in which the entire diagram has been examined. In the paragraphs that follow, the portions of these diagrams that are most relevant to soldering technology–primarily, vertical sections (isopleths), which extend from important solder alloy compositions to increasing amounts of substrate elements are

discussed. Consult the original references shown in Table 1 for a more comprehensive discussion of these diagrams.

Table 1. Survey of relevant ternary equilibrium phase diagram studies. Alloy compositions are shown in wt.%.

System	Reference	Complete Diagram?	Comments
Au-Sn-Pb	26	no: liquidus surface for AuSn-Pb-Sn diagram.	Vertical sections through AuSn-Pb-Sn space model at 10wt.% Au and 10, 30 and 50wt.%Pb. Also,portions of vertical section from 40wt.%Pb-60Sn toward Au corner
Au-Sn-Pb	27	yes: complete liquidus projection and 63Sn-37Pb/ Au isopleth.	Reaction isotherms included.
Au-Sn-Pb	28, 29	no: AuSn-Pb pseudobinary; liquidus-liquidus projection of Au-AuSn-Pb portion, and several Au-rich isopleths	Redetermination of Au-AuSn-Pb portion of Au-Sn-Pb system.
Au-In-Pb	30	no: $AuIn_2$-In-Pb portion	Quasibinary Pb-$AuIn_2$ and Pb-AuIn diagrams. Au-50wt.%In-50Pb isopleths also developed.
Au-In-Pb	31	no: Pb-AuIn quasibinary diagram.	Comparison of diagram with that of previous study: disagreement on monotectic temperature.
Au-In-Pb	32	no: Au-50wt.%In-50Pb isopleth.	Correction to this isopleth since previous diagram [30] included nonequilibrium $\alpha 1$ phase.
Au-In-Sb	33	no: AuIn-Sb isopleth	Eutectic temperature between AuIn and Sb at 421°C.
Cu-Sb-Pb	34	yes: complete liquidus projection.	Survey of previous work on this system. The Pb-rich corner may not be correct, since existing diagram is based on a now outdated Cu-Sb binary diagram.

Table 1. Survey of relevant ternary equilibrium phase diagram studies (cont'd.)

System	Reference	Complete Diagram?	Comments
Cu-Sn-Pb	34	yes: complete liquidus projection.	Survey of previous work on ternary phase diagrams for this system.
Cu-Sn-Pb	35	yes: complete liquidus projection and activity diagrams.	Survey of data on both ternary equilibria and activity data for this system.
Cu-Sn-Pb	36	no: low Cu additions to Pb-Sn	Differential scanning calorimetry experiments confirm the existence of a ternary Cu-Sn-Pb eutectic at low Cu composition, with eutectic temperature of 182°C (1°C below Pb-Sn eutectic temperature).
Cu-Sn-Pb	37	no: liquidus projection and crystal structure of 44 ternary alloys, Pb-10-90wt.%Sn-0.2-2wt.%Cu.	Ternary eutectic at approximately 60.9-61wt.% Sn-38.8Pb-0.2-0.3Cu was observed.
Cu-Sn-Pb	38	no: low Cu portion of 60wt.% Sn-40Pb/Cu isopleth.	Quasibinary eutectic solder composition of 0.23wt.% Cu + bal. 60Sn-40Pb was identified, with eutectic temperature of 181°C.
Ni-In-Sn	39	yes: complete diagram at 700°C	Continuous intermetallic phase field between Ni_3In and Ni_3Sn as well as between Ni_3In_2 and Ni_3Sn_2.
Fe-Pb-Sn	40, 41	no: Sn-0-50wt.%Pb melts with additions of Fe.	Solubility of Fe in Sn-Pb alloys decreases as Pb content is increased. Solubility data generated over temperature range 250° to 800°C.

The Au–Sn–Pb system has been more completely characterized over a wide range of temperatures than any of the other systems shown in Table 1. It is interesting to note that all of the phase diagram studies for both the Au–Sn–Pb and Au–In–Pb systems have apparently been driven by the need to fully characterize alloy systems that are important for electronic materials applications. Karnowsky and Rosenzweig [27] determined liquidus temperatures over the entire phase diagram, and developed a vertical section (isopleth) from eutectic Sn–Pb solder to 90wt.% Au. Figure 5a shows the dilute Au portion of this isopleth. Note that while a significant amount of Au can be dissolved into molten eutectic 63Sn–37Pb alloy, there is fairly limited solid solubility for Au. As a result, the $AuSn_4$ intermetallic compound is commonly observed to form during solidification. This compound has a distinct needle-like morphology, and if present in significant volume fractions, can embrittle the solder alloy.

The relatively high solubility of Au in the eutectic 63Sn–37Pb alloy is in distinct contrast to the Au–50Pb–50In system. The Au–50Pb–50In vertical section, as determined by Marcotte and Ricker [32], is shown in Figure 5b. Note that the solubility of Au in liquid 50Pb–50In solder is substantially less at soldering temperatures of interest (225 to 260°C) compared to the solubility of Au in 63Sn–37Pb alloy. A technologically important consequence of this difference is that for identical times above the solder alloy liquidus, there is significantly less Au dissolved into 50Pb–50In solder compared to the 63Sn–37Pb alloy. This is especially important in the case of thin film circuitry, where the "leaching" characteristics of 63Sn–37Pb against Au substrates usually precludes the use of this alloy. In general either Pb-rich Pb–Sn or 50Pb–50In alloys are commonly used for these applications.

In contrast to the Au–Sn–Pb and Au–In–Pb ternary systems, work on the Cu–Sn–Pb system apparently preceded extensive electronic applications. Both Hoffman [34] and Chang [35] have summarized previous work on this system, which extends back to the early part of this century. Recent work on this system has concentrated on the dilute Cu sections of this diagram–those compositions relevant to soldering technology. Marcotte and Schroder [36] used differential scanning calorimetry to identify the effect of small additions of Cu on eutectic Sn–Pb as well as the effect of small additions of Sn to the Pb–Cu eutectic. Their results on the Sn–Pb eutectic with dilute Cu additions are consistent with the recent investigations of Pikunov, et al. [37] and Okamoto and Yasuda [38]; a ternary Cu–Pb–Sn eutectic exists near the binary Sn–Pb eutectic, with a eutectic temperature 1 to 2°C below 183°C (Sn–Pb eutectic temperature). While the exact ternary composition has not been determined, it is apparently at a fairly low Cu composition. For example, in the partial vertical section that Okamoto and Yasuda [38] developed, shown in Figure 5c, the Cu composition at the eutectic temperature is 0.23 wt.%. Unfortunately, a systematic study that has determined the solid solubility limits of Cu in commercial solder alloys has not been reported. That is, how much Cu can be dissolved into these alloys before the Cu_6Sn_5 intermetallic phase is formed in the solid state is not known. One would assume that Cu has a low solubility in Sn–Pb alloys, since for the case of the binary alloys, only 0.9 and <0.007 wt.% Cu can be dissolved into pure Sn and Pb, respectively [21]. It is reasonable to assume that it is much more difficult to embrittle a solid 60Sn–40Pb solder joint with Cu additions compared to the case of Au additions.

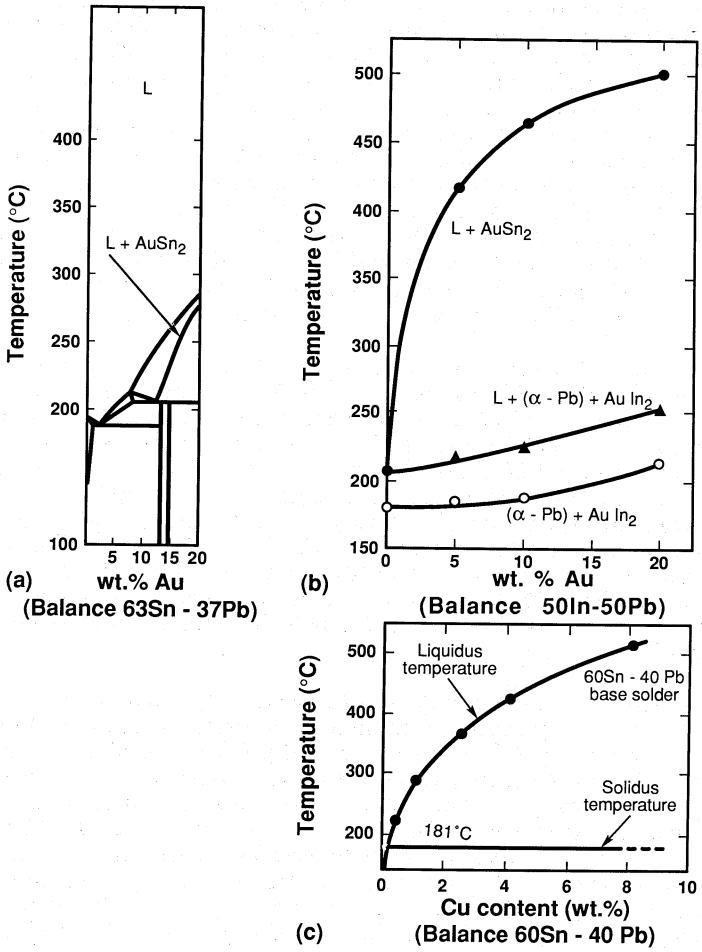

Figure 5 Vertical sections of important solder alloy-substrate metal ternary phase diagrams. (a) Dilute Au portion of 63wt.%Sn–37Pb/Au vertical section of Au–In–Pb ternary system [27, 49]. (b) Dilute portion of 50wt.%In–50Pb/Au vertical section of Au–In–Pb ternary system [32]. (c) Dilute Cu portion of 60wt.%Sn–40Pb vertical section of Cu–Sn–Pb ternary system [38].

It is instructive to compare the vertical section of the Cu–60Sn–40Pb system above the eutectic temperature, shown in Figure 5c, with that of the Au–Sn–Pb system (see Figure 5a). Note that for soldering temperatures of interest (220 to 260°C), a substantially lower amount of Cu can be dissolved into near eutectic Sn–Pb alloy relative to Au.

While the work on the Fe–Sn–Pb system is confined to the dilute Fe portion, the results of these studies [41, 42] are nevertheless important. Eremenko et al. [41]

demonstrated that the solubility of Fe in Sn–Pb alloys decreases substantially as Pb additions are made. The fact that Fe has generally low solubility in these alloys suggests that Fe may be able to serve as an effective diffusion barrier in protecting higher solubility substrate materials such as Au. Although analogous data has not been generated in the case of Ni–Pb–Sn, one would suppose that Pb additions to Sn would have similar effects on Ni solubility in these melts.

KINETICS OF SOLDER/SUBSTRATE REACTIONS: THE EMPIRICAL APPROACH

While the equilibrium phase diagrams can be used to indicate what phases can form, the kinetics of solder–substrate reactions determine the structure of both the solder–substrate interface and the amount of substrate that is dissolved into the solder alloy. When considering the design of solder–substrate systems for high reliability applications, two separate problems must be considered:

- The amount of scavenging (dissolution) of the substrate by the solder that can occur during both solder processing and rework. It is important to note that some of the substrate may be dissolved into the molten solder, and may then form an intermetallic compound dispersoid within the solid solder joint (such as $AuSn_4$ in 60Sn–40Pb solder) during solidification.

- The amount of intermetallic compound(s) formed in the solid state in the solder alloy-substrate interfacial region. Intermetallic compounds may form both as a result of solder components diffusing into the substrate and forming a continuous layer of intermetallics during the soldering operation (such as Cu_6Sn_5 formation when Sn-rich solders are used with a Cu substrate) or during subsequent aging during service.

It is often assumed that it is simple to characterize the amount and morphology of intermetallics formed as a result of solder processing. However, even in the case of as-fabricated solder joints, one needs to carefully characterize the amount of intermetallic compounds resulting from both initial processing and rework (if any), as well as the relative amount of substrate material remaining. The latter point is very important in the case of thick-film hybrid microcircuits, where a certain percentage of the solder pad is consumed as a result of molten solder processing. In this case, one is usually dealing with a limited amount of substrate material (rarely in excess of 25 μm) the thickness of which may vary from lot to lot. The situation is actually better for the case of thin film hybrid microcircuits, since these systems usually employ a diffusion barrier system (such as Ti/Pd or Cr) between the solderable (usually pure Au) layer and the ceramic substrate.

Solid-state growth of intermetallics during service poses a more difficult reliability problem. Over the course of service life, intermetallic layers may grow to significant thicknesses (>20 μm) depending on the kinetics of growth for a particular solder–substrate system and the service conditions (cumulative time at temperature), especially at temperatures above ambient. For the case of long-life components used in critical applications, it is generally not possible to age a solder joint for the exact thermal conditions that it will experience over its

service life, since the projected life of the component containing the solder joint may be as long as 20 to 30 years for some military applications. Thus, it is usually necessary to employ accelerated aging conditions in order to determine whether or not the amount of intermetallic encountered in service will compromise performance. As is discussed later in this chapter, to have accelerated aging conditions accurately approximate actual service conditions, it is important to verify that the same growth mechanism which operates at the service temperature also occurs at the accelerated aging temperatures. This is the only way that a proper time extrapolation can be performed.

The following two sections present surveys of the engineering literature that focus on the respective problems of molten solder–substrate reactions and solid-state growth of intermetallic compounds.

Molten Solder–Substrate Reactions

During wetting, molten solder reacts with the solid substrate. As mentioned previously, two processes are observed to occur simultaneously: the base metal dissolves into the molten metal, and the active constituent in the solder combines with the base metal to form intermetallic compounds on the surface of the base metal. The relative amount of base metal that goes into solution is, of course, related to its solubility in that particular solder, while the intermetallic compound formation at the surface depends more on the solubility of the active element in the base metal. Both processes obviously also depend on the time spent above the solder's liquidus temperature. Note also that additional intermetallics may form in the solder joint as the solder solidifies since the solid solder may be supersaturated with the base metal (see Figure 5a).

The reaction between the molten solder and substrate surface is very important because it plays a major role in determining the microstructure of the solder joint. Clearly, there are a number of parameters (such as time, temperature and surface cleanliness) that must be optimized to produce a high-quality solder joint. Dissolution of the metallized layer may result in de-wetting due to exposure of an unsolderable substrate surface. A solder joint may become embrittled if excessive amounts of intermetallic are formed in the bulk solder joint during cooling and solidification. Finally, intermetallics that have grown at the molten solder-base metal interface could lead to loss of strength at this interface under certain loading conditions.

A number of studies have been published that explore the molten solder-solid substrate reaction; these studies are summarized in Table 2 [38, 42–51]. Many of the studies shown in Table 2 have examined the radial dissolution of wires in a molten solder pot (conditions where the mass of the solder is much greater than that of the wire). For the radial geometry, the data are observed to follow a linear growth law combined with an Arrhenius factor as follows [44]:

$$-\Delta r = r_0 - r(t,T) = t\, c\, e^{-Q/RT} \qquad (2)$$

where r(t,T) is the radius remaining after a given time t at temperature T (Kelvin), r_0 is the initial wire radius, and c exp(–Q/RT) is the linear dissolution rate.

The dissolution of Au in Sn-based solders has been extensively studied [44, 45, 48, 49]. Au has good wetting characteristics and therefore is an excellent solderable protective metallization. The diffusion rate of many elements (e.g. the elements beneath the Au metallization as either the bulk material or a barrier layer) trough the Au is slow enough so that oxide film formation on the surface takes place very slowly. The dissolution of Au into molten Sn-based solder is extremely rapid, and the higher the temperature of the molten liquid the faster the dissolution [44,48]. The explanation for the rapid dissolution is that the Au is highly soluble in molten Sn [45,49], which creates a large driving force to diffuse the Au into the solder.

The intermetallic that forms on reaction of the molten Sn and Au is $AuSn_4$. The intermetallic is found both at the solder/Au interface as well as in the bulk of the solder joint. This intermetallic phase tends to have an acicular morphology and it must be emphasized that relatively small weight percentages of Au dissolved into the eutectic 63Sn–37Pb solder alloy can lead to significant volume fractions of Au–Sn intermetallic phases. Previous work on the Au–Sn–Pb ternary system (see Figure 5c) indicated that significant amounts of $AuSn_4$ form in a ternary of 6wt.%Au–35Pb–59Sn [26], while even 1 wt.% Au added to 63Sn–37Pb alloy results in a detectable amount of $AuSn_4$ [52]. Bester [53] showed that additions of >4 wt.% Au to 63Sn–37Pb solder significantly reduces the impact strength of these alloys. Brittle tensile behavior is observed in bulk mechanical test specimens of eutectic Pb–Sn alloys with $\geq$7.5wt.% Au additions [52].

Table 2. Dissolution rate studies: molten solder alloys with solid substrates. Alloy compositions shown are in wt.%. (References are presented in chronological order.)

Reference	Solder Alloy(s)	Substrate(s)	Comments
42	30Sn-70Pb, 15Sn-85Pb and 2Sn-1.5 Ag-96.5Pb	70Cu-30Zn(α-brass)	Dissolution of brass foil occurred by formation of a ternary Cu-Sn-Zn reaction product, reaction with high Pb alloy most sluggish. Cu_6Sn_5 was observed to form under certain conditions. Reaction process found to be rate controlled by diffusion of Sn from solder into brass.
43	Sn, 63Sn-37Pb, 30Sn-70Pb, 15Sn-85Pb, 5Sn-95Pb, 1Sn-2Ag-97.5Pb and Pb	Cu Alloys: C102, C129, C143, C194, and C260*	Higher reaction rates occur with Sn rich solders. Slowest reaction rate was for Cu-Cd and Cu-Ag alloys (C143 and C129, respectively Agitation of solder increases the reaction rate.
44	60Sn-40Pb	Au, Ag, Cu, Pd, Pt and Ni	Order of substrates is in increasingly sluggish dissolution rate (Au fastest, Ni slowest)
45	5Sn-95Pb and 5In-2.5Ag-92.5Pb.	Au, Ag, Cu and Ni	Same ranking order as [44].
46	60Sn-40Pb, 63Sn-37Pb, 60Sn-2Cu-38Pb, 60Sn-4Ag-36Pb and 63Sn-1.5Ag -38.5Pb.	Ag and Cu	Effect of Ag and Cu additions to Sn-Pb solder on dissolution rate of Ag and Cu wires, respectively. Addition of Ag or Cu to the solder helps to decrease dissolution rate of Ag or Cu wires.
47	60Sn-40Pb, 30Sn-70Pb, 20Sn-80Pb, 10Sn-90Pb,14Sn-6Sb-80Pb, 3Sn-2.25Pb-94.75Pb, 1Sn-1.5Ag-97.5Pb and alloys with low Cu additions.	Cu	Kinetics study showed that high Pb low Sn solders, along with 60Sn-40Pb and 70Sn-30Pb with Cu additions, have slowest dissolution rates.

Table 2. Dissolution rate studies: molten solder alloys with solid substrates. Alloy compositions shown are in wt.%. (cont'd)

Reference	Solder Alloy(s)	Substrate(s)	Comments
48	Sn, 60Sn-40Pb, 93Sn-7Au, 60Sn-4Au-36Pb, 53Sn-17.5In-29Pb-0.5Zn and 49Sn-18Cd-33Pb.	Au	Dissolution of 1-mm diameter Au wires as a function of temperature. Sn-Cd-Pb allow found to have slowest dissolution rate as a function of temperature.
49	50In-50Pb and 63Sn-37Pb	Au	Au dissolution much less in molten 50Pb-50In, can be explained via pseudobinary phase diagrams.
50	60Sn-40Pb	Au, Ni	High-temperature x-ray diffraction study, which permits Avrami plots to be constructed to illustrate reaction of solder with foil substrates. Relative results were consistent with those of Bader [44].
38	60Sn-40Pb and 60Sn-40Pb and additions.	Cu	Erosion rate of 50 to 70 μm diameter up to wires measured from 200 to 400°C.Time to fully consume Cu wire increases with higher wt.% Cu relative to baseline solder, with maximum increase at lower temperatures.
51	20Sn-80Au	Cu	Reaction rate is rapid until Cu is saturated in molten solder. Cu Solubility in molten 80Au-20Sn is ~10wt.% at 395°C.

* Copper Development Association designations for Cu alloys. Consult *CDA Standards Handbook -Volume 2:Wrought Products* (Copper Development Association, Greenwich, CT) for exact compositions.

With the rapid dissolution of Au and possible joint embrittlement with Sn-based solders, the amount of Au used for metallizations has to be limited for thick-film electronic applications where 63Sn–37Pb is used. In fact, Au is usually alloyed with elements such as Pt and Pd to significantly slow the dissolution kinetics. However, there are applications where thin Au films, deposited either by means of vapor deposition or plating, are used in conjunction with diffusion barriers. In these cases Yost [49] has shown that the use of In-based solders (typically 50In–50Pb) dramatically reduces the dissolution rate of Au into the molten solder. This

reduction is attributed to the smaller solubility of Au in the molten 50In–50Pb alloy (see Figure 5b). The intermetallic that forms on reaction between Au and 50In–50Pb is $AuIn_2$, and there is some evidence [49] that interfacial layers of this compound resulting from soldering operations are not inherently brittle insofar as they contain an interspersed layer of Pb.

Studies on other precious metal coatings have shown that Ag and Pd behave similarly to Au [44]. Their dissolution rates in Sn-based solders are somewhat slower but still significant. Note that the formation of interfacial intermetallics between the molten solder and the precious-metal base has little influence on the dissolution rate [44]. Both Sn and Au can rapidly diffuse through the intermetallic. Also, the intermetallic layer can easily spall off thereby creating new surfaces for dissolution–intermetallic formation to take place.

Base metals such as Ni, Cu, and Pt have much slower dissolution rates than precious metals such as Au, with Ni being the slowest [44, 45]. Figure 6 shows the radial dissolution rates for Au, Ag, Cu, Pd, Pt and Ni wire as a function of temperature [54]. In general, the dissolution of these base metals is a function of Sn-content; the greater the percentage of Sn, the faster the dissolution. Work by Okamoto and Yasuda [38] showed that, for Cu, the initial dissolution into molten 60Sn–40Pb is rapid until the solder has reached Cu saturation and then dissolution slows dramatically. The extent of embrittlement of solder joints by (Cu, Ni, or Pt)–Sn intermetallics has not been studied systematically, but is probably less than that with Au. A study by Howes and Saperstein [43] on Cu showed that adding small amounts of Ag or Cd to the solder slowed dissolution. They attributed this to the formation of a coherent Ag–Cd–Sn intermetallic at the solder-base metal interface that acts as a diffusion barrier to the Cu.

The mechanisms involved during the molten solder-solid base metal reactions have not been explored in great detail. Lommel and Chalmers [55] addressed dissolution of a solid metal into a liquid. The major assumption in this work was that no compounds (intermetallics) form at the liquid/solid interface to inhibit growth. They found that when growth follows a $(Dt)^{1/2}$ function the rate limiting step was diffusion of the liquid element into the solid metal.

When an intermetallic compound forms at a liquid solder-solid substrate interface, the limiting steps can be more complex:

- Diffusion of the base metal and solder through the interfacial intermetallic.
- Diffusion of the reacting species (Sn in Sn–Pb solder) through the molten solder to the reaction interface.

The morphology of the intermetallics that form between molten solder and the base metals can be related to dissolution. The slower the dissolution rate the more planar the interfacial intermetallics that form. This can be observed qualitatively in the micrographs shown in the work by Bader [44] and Howes. Saperstein and Howes [43] studied 60Sn–40Pb on brass and submit that the reaction that occurs is one or both of the following:

- The Sn reacts with the brass to form a low-melting-temperature eutectic that dissolves into the solder and upon subsequent cooling forms in the solder.
- The interfacial intermetallic layer is brittle and fractures off into the molten solder, exposing new surfaces for intermetallic growth. These fractures occur due to internal stresses that arise on the phase transformation that creates the intermetallic.

Frear et al. [56] postulated, based on observations of 60Sn–40Pb solder in contact with a Cu substrate, that whiskers of Cu_6Sn_5 intermetallic form at the interface between the solder and the Cu and grow out into the molten solder. The whiskers break off and partially dissolve into the molten solder. This is consistent with the observation that stirring the molten solder promotes dissolution of base metal [43] because more fresh surface is created when the whiskers break off.

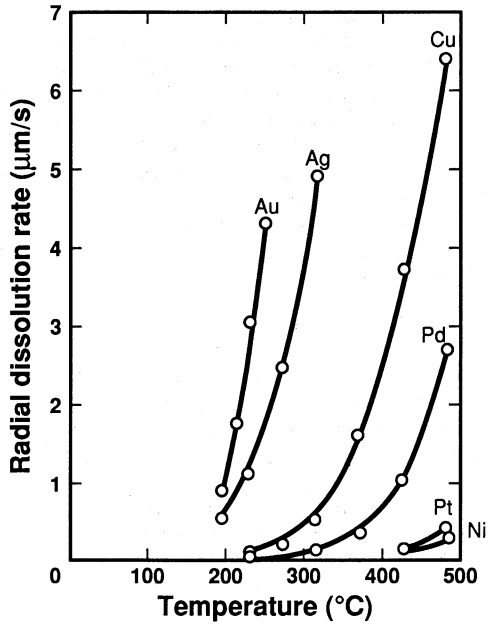

Figure 6 Radial dissolution rate of metal wires in 60wt.%Sn–40Pb solder alloy at various temperatures [54].

Solid-State Growth of Intermetallic Compounds

The solid state growth of intermetallic compounds is generally a more complex engineering problem than intermetallics which grow during or are precipitated out as a result of a soldering operation. There are two broad areas of concern:

- The growth of intermetallic layers such as $NiSn_3$ or Cu–Sn intermetallics on pretinned substrates that can be difficult to wet in subsequent soldering operations.

- The long-term growth of intermetallic layers at the solder–substrate interface during the service life of the solder joint.

The latter case is more insidious because over long periods of time these layers can grow to significant thicknesses (>20 μm) and the solder–intermetallic interface may constitute easy sites for crack initiation and propagation.

There are a number of electronic applications where the solid-state growth of intermetallics is undesirable. One important situation has already been discussed: the problem of intermetallic growth on pretinned parts during storage, which leads to a situation where parts are not solderable. If, for example, a nonequilibrium intermetallic phase has grown [20], it may be possible to heat the pretinned part in order to decompose the metastable phase, and hopefully restore solderability. Often, as in the case of pretinned Cu parts that have grown Cu_3Sn, it may be extremely difficult to restore solderability without the aid of an aggressive flux. With respect to parts in service, problems have been encountered at Sandia National Laboratories with excessive solid-state intermetallic growth in thick-film Au substrates that have been soldered to as well as in situations where intermetallic growth prevented thermal fusing action. The growth of intermetallic layers also leads to a volume increase in the solder joint because the intermetallics are not closely packed structures. There are usually two options that can be used to inhibit solid-state growth of intermetallics: (1) change either the solder alloy or substrate material so that that the system exhibits generally slower intermetallic growth kinetics, or (2) use diffusion barriers to inhibit the growth of intermetallic layers.

For engineering purposes, one is frequently interested in predicting the intermetallic thickness that may grow explicitly as a function of time at temperature. The basic data and predictive relations presented in this chapter deal with intermetallic growth at a planar interface; refer to Janco and Braun [57] for a the treatment of a cylindrical geometry appropriate for solid state growth of intermetallics on a base metal wire. In many cases, it is appropriate to use the following empirical relation to predict the total intermetallic thickness as a function of time and temperature:

$$x(t, T) = x_0 + A\ t^n\ e^{-Q/RT} \qquad (3)$$

where x is the total intermetallic thickness at time t and temperature T (Kelvin), x_0 is the thickness of the intermetallic in the as-soldered condition (at t=0), A and n are constants, R is the universal gas constant, and Q is the apparent activation energy for a particular growth process. A, n, and Q are constants that can be obtained by means of multivariable linear regression analysis. To correctly apply Equation 3, the same growth mechanism determined at the higher temperatures for the accelerated aging conditions must also apply at lower temperatures.

It is useful to distinguish between the following two types of solid–state growth based on the value of the time exponent n:

- *n = 1, Linear Growth Kinetics.* Phenomenologically, linear growth implies that the growth rate is limited only by the reaction rate at the growth site (e.g. solder/substrate interface). That is, the growth is not limited by the rate at which the constituents of the intermetallic compound are able to diffuse to the reaction site. This situation is the easiest to deal with mathematically, because Equation 3 defines the equation of a straight line; the reaction rate $\beta = dx/dt$ is thus independent of time and is given by A exp(-Q/RT). In general, many solder–substrate systems that are fairly reactive can be represented by the linear growth law. Examples include Au in contact with many different Sn–In–Pb solder alloys [58], Au in contact with 50In–50Pb alloy [59], and Cu in contact with the 50Sn–50In alloy [24, 25].

- *n = 1/2, Parabolic Growth Kinetics.* Parabolic growth kinetics apply when layer growth is controlled by bulk diffusion of elements to the reaction interface. Growth of the intermetallic layer becomes increasingly difficult as the layer grows because diffusion of one or more of the intermetallic constituent elements must diffuse through the existing intermetallic layer to reach the reaction site. For the case of ideal parabolic kinetics, the growth rate (dx/dt) is proportional to $A\ t^{-1/2}\ \exp(-Q/RT)$; hence, the growth rate declines as time and the diffusion distances increase. Examples of important systems where the intermetallic growth rate is often *represented* as parabolic include Cu and many Cu alloys in contact with Sn and Sn–Pb solders [60].

Note that in actual practice, when data are analyzed using the generalized kinetic growth law (Equation 2) many systems that are presumed to exhibit parabolic growth kinetics actually have subparabolic kinetics ($n<1/2$). For example, this is true for the case of Cu in contact with either pure Sn or the 60Sn–40Pb alloy, where the actual time exponents observed when data is analyzed with Equation 3 are 0.35 and 0.37, respectively [61]. This behavior is illustrated in the micrographs shown in Figure 7. Subparabolic growth behavior can be rationalized in the case of Cu or Cu alloys in contact with Sn and Sn-rich Sn–Pb alloys because two intermetallic compounds, Cu_6Sn_5 and Cu_3Sn, are observed to grow in the solid state. The Boltzmann transformation which is used to derive the parabolic growth relationships assumes molar volume constancy within the system. The assumption of molar volume constancy is not always valid when intermediate phases of vastly different crystal structures form, such as in the formation of intermetallic compounds between solders and substrates. The absence of molar volume constancy during the growth process is most likely responsible for growth rates which appear to be subparabolic. Unfortunately, a quantitative multilayer growth formalism which includes the effect of variable molar volume has not yet been developed. In the absence of a long-term database for intermetallic growth in a particular system, one may have to assume that n = 1/2 in order to make long-term predictions regarding intermetallic layer growth if it is apparent from short term data that n is close to 1/2.

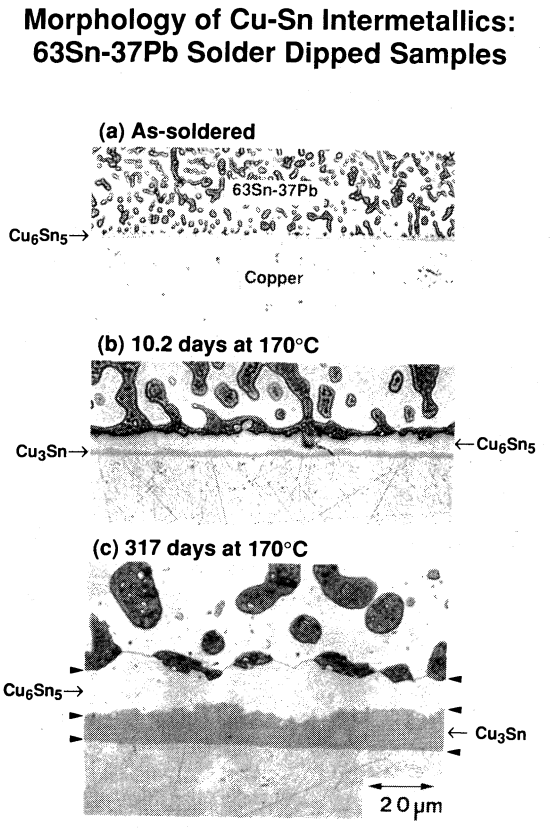

Figure 7 Morphology of Cu–Sn intermetallic compounds. All three optical micrographs (1000X prior to reduction for printing) are from OFHC–Cu samples that were dipped in 63Sn–37Pb solder alloy. (a) As-soldered condition: only Cu_6Sn_5 compound is resolved. (b) Sample aged for 10.21 days at 170°C: both Cu_6Sn_5 and Cu_3Sn are apparent. (c) Sample aged for 300 days at 170°C. Note that Cu_3Sn is apparently growing at the expense of the Cu_6Sn_5 layer.

From an engineering point of view, for long-term applications it is desirable to have a solder–substrate system with Q and n as low as possible. Unfortunately, there are often other design or production requirements (or both) in microelectronics that drive the materials selection process.

The following sections present a survey of previous solid-state intermetallic growth studies grouped according to the type of base metal substrate that was investigated: Au and Au alloys, Cu and Cu alloys, and other substrate metals, such as Ag, Ni, or Fe. These paragraphs are followed by a brief discussion of the experimental methods used to characterize the solid-state growth of intermetallics.

The Formation of Kirkendall Porosity

The diffusional processes which produce the intermetallic layers require that all elements in the solder joint (i.e., Cu and Sn) will diffuse. If one element diffuses more quickly than the other, excess vacancies will be formed in the material with the highest diffusion rate. These excess vacancies will eventually accumulate and coalesce in a compositional plane defined by the relative diffusional fluxes. The result will be a line of voids (e.g. porosity). In the literature, this effect is known as Kirkendall porosity. It becomes especially severe in cases where the volume of one material is very small relative to the second material. For example, when a very fine wire is attached with a relatively large volume of solder. If the diffusional fluxes are such that the Kirkendall porosity forms in the thin wire a severe reliability problem may result. The porosity may reduce the cross-sectional area of the wire sufficiently so that it is mechanically weakened. In the area of packaging, this problem is actually more severe for wire bonding. If fine Al wires are bonded (thermocompression, ultrasonic) to Au contact pads, a diffusional reaction will create Au–Al intermetallic compounds and Kirkendall voids in the Al wire. The wire, with its cross-sectional area now reduced by the porosity, has greatly reduced mechanical strength. The intermetallic compounds and the pores give the joint a purple hue and the defect is therefore often called *the purple plague*.

STUDIES OF SOLID STATE INTERMETALLIC GROWTH

Au and Au Base Alloys

The solid-state intermetallic growth kinetics have been investigated for a wide variety of solder alloys in contact with both pure Au and Au alloy substrates. A chronological survey of these studies is presented in Table 3 [57–59, 62–66]. It is useful to first consider the situation of pure Au in contact with various solder alloys [57–59, 62, 63, 65]. Pure Au generally reacts quite readily with all of the solder alloys that have been studied, at temperatures in excess of 70°C. It appears that in virtually every case, linear reaction kinetics are observed. Unfortunately, the authors are not aware of any work where the reaction rate of pure Au with Pb-rich alloys has been documented. One would expect fairly sluggish reaction kinetics in such alloys; however, these Pb–rich solder alloys are generally not as readily wettable to many substrate surfaces.

Table 3. Chronological summary of intermetallic growth studies: solders on Au and Au alloy substrates. All compositions shown are in wt.%. Samples were prepared by solder dipping unless otherwise indicated.

Reference(s)	Solder Alloy(s	Substrate(s)/ Form	Comments

57, 58, 62	37.5 Sn-25In-37.5 Pb, various Sn-In-Pb-Zn Sn-In-Pb-Cd, and Pb-Sn-Au alloys; 37.6 Sn-35Pb-21.1Cd-6.5Sb, and 37.6Sn-35.2Pb -21.2Cd-6Bi.	Au wire	Solid-state reaction of up to 40 μm diameter Au wire with various solders. 37.5Sn-25In-37.5Pb alloy studied extensively; reacts slower with Au than 60Sn-40Pb alloy. Slowest reaction rate at 110°C for solders considered is a 53Sn-17.5In-29Pb-0.5Zn alloy [58].
63	Sn, 63Sn-37Pb (diffusion couples)	Au foil	After 300 hr, 10 μm of Au foil is consumed by 63Sn-37Pb at 121°C while entire 75 μm Au foil is consumed by pure Sn at 195°C. AuSn, $AuSn_2$ and $AuSn_4$ were resolved for Au/Sn, while the latter two only were observed for Au/63Sn-37Pb sample.
64	95Sn-5Ag, 1Sn-97.5Pb-1.5Ag	Au-Pt thick film (grade not specified)	Samples ages 85°, 125°, and 150°C up to 200 h. Parabolic growth relation was assumed and correlations show that the reaction rate for Sn-Pb-Ag solder is much more sluggish than for Sn-Ag alloy. $AuSn_4$ reaction product observed using energy dispersive analysis
65	50In-50Pb	Au: both evaporated thin film and 75 μm thick foil.	Thin-film Au samples aged 70° to 170°C, exhibited two phase reaction layer of Au_9In_4 and $AuIn_2$. A variety of growth kinetics equations were examined: linear growth kinetics relation found to give reasonable fit to data. Foil Au sample evaluated at 150°C, early times agree with thin film data, but extended aging times show a single phase layer of Au_9In_4 adjacent to Au foil.

66	63Sn-37Pb, 62Sn-36Pb-2Ag and 50Pb-50In (solder creams with mildly activated rosin flux, 12 vol% loading)	Au-Pt thick film alloy.	Intermetallic growth rate for Au-Pt at 135°C for both solders is roughly a factor of 10 slower than for pure Au/50Pb-50In results of Yost et al. Linear and parabolic relations were examined; both appear to give a good fit to the data. (Authors present results of linear fit to the data)
59	50In-50Pb	Au thick film, Au-3Pd thick film alloy.	Long term growth studied at 70 to 170°C for up to 5000 h. The intermetallic growth rate for Au-3Pd thick film is significantly less than for pure Au thick film, especially at lower (~70°C) temperatures. Linear kinetics law works well for both data sets.
67	63Sn-37Pb	Au-Pt-Pd thick film alloy.	Preliminary results up to 500 h at 70 to 170°C. Kinetics are apparently parabolic and sub-parabolic, depending on temperature. A mixed (Au, Pt, Pd)$_1$Sn$_4$ intermetallic compound is the reaction product.

Braun [58] examined the solid-state intermetallic growth kinetics at 110°C for a variety of soft solder alloys in contact with pure Au wire. Note that the 60Sn–40Pb alloy has most rapid reaction rate with the Au wire. When a ternary 37.5Sn–25In–37.5Pb solder alloy was examined, the primary constituent of the reaction phase was found to be $AuIn_2$. The slowest consumption of the Au wire was observed with the quaternary 53Sn–17.5In–29Pb–0.5Zn alloy. Braun suggested that Zn additions aided in slowing the diffusion of the solder constituents to the reaction site.

Robertson and Karnowsky [63] investigated the interdiffusion of Au with pure Pb, pure Sn and 63Sn–37Pb solder using diffusion couples at the respective temperatures of 121°, 195°, and 121°C. Samples were examined using wavelength dispersive electron microprobe analysis. Negligible diffusion was observed in the Pb–Au diffusion couple after 288 h at 121°C. All three intermetallic compounds–AuSn, $AuSn_2$ and $AuSn_4$ were observed in the Sn–Au diffusion couple. For the case of 63Sn–37Pb at 121°C, both $AuSn_2$ and $AuSn_4$ were observed, with the latter phase exhibiting Kirkendall porosity. A Pb-rich layer was observed to build up adjacent to the $AuSn_4$ phase, and the authors suggest that this layer may serve to slow the reaction rate. While this may be true, it

should be emphasized that the Pb rich phase cannot be a perfect diffusion barrier since significant amounts of Sn (up to 19 wt.% at the eutectic temperature [21]) are soluble in this phase. The $AuSn_4$ phase was observed to be considerably thicker than the $AuSn_2$ phase, and the authors concluded that the $AuSn_4$ phase ought to dominate in the case of limited amounts of Au.

The solid-state reaction of Au with 50Pb–50In alloy has been characterized extensively over a wide range of temperatures [59, 65]. Yost et al. [65] investigated the reaction of 50In–50Pb with evaporated Au films over the temperature range 70° to 170°C. A two-phase $AuIn_2$–Pb layer constituted virtually all of the reaction layer, although a thin layer of Au_9In_4 was observed immediately adjacent to the Au. The authors examined the thickness, time, and temperature data using a variety of kinetic laws, and found that a linear growth law produced the most consistent predictions over a wide variety of temperatures. Figure 8 shows a plot of the intermetallic thickness as a function of time at 85°, 110°, 130°, and 160°C.

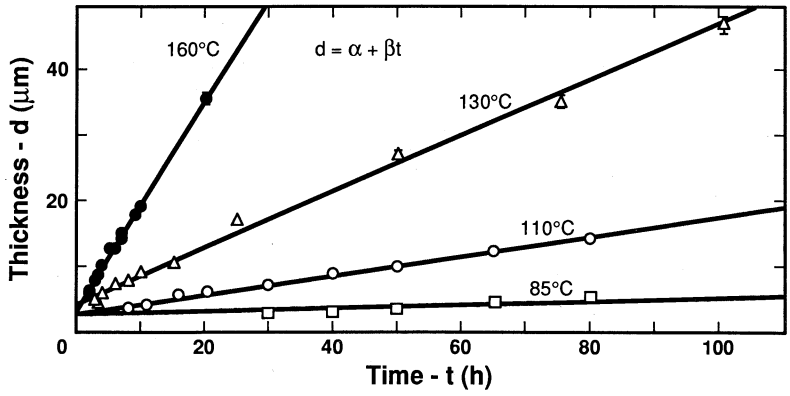

Figure 8 Kinetics of intermetallic growth at 85°, 110°, 130°, and 160°C for evaporated Au in contact with 50In–50 Pb solder alloy [65].

In general, considerably slower intermetallic growth kinetics can be observed with judiciously selected alloying additions to the Au. A comparison of the linear growth rates obtained between pure Au thick film in contact with 50In–50Pb alloy and an Au–3wt.%Pd thick film alloy in contact with the same solder is shown in Figure 9. Note that the apparent activation energy (the slope of the Arrhenius plot) for the Au–3Pd alloy is significantly higher than for the pure Au thick film; this leads to a situation where the growth rate for the alloyed Au thick film is significantly slower than for the pure Au at lower temperatures (such as 70°C), which are similar to the maximum temperature expected during service for these solder joints.

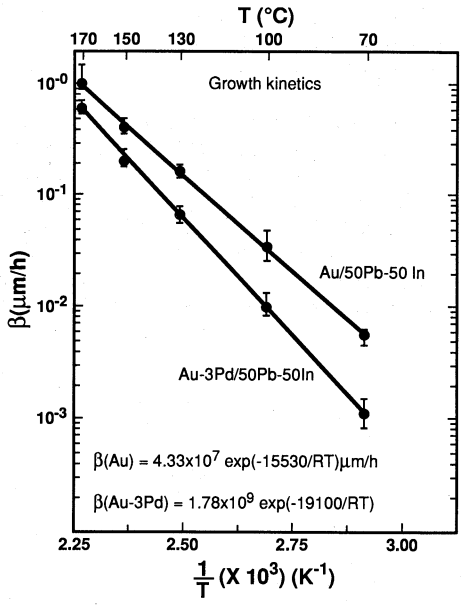

Figure 9 Arrhenius plot of the linear growth rate for thick-film Au/50In–50Pb and Au–3Pb/50In–50Pb systems [59].

More highly alloyed Au thick-film alloys (the "Pt–Au" alloys) have been observed to exhibit even more sluggish intermetallic growth rates [66]. Unfortunately, formulation of these various "Pt–Au" inks are proprietary information, and consequently the exact composition of the thick film alloys themselves cannot be disclosed. Sulouff [64] characterized the reaction kinetics between a thick film Pt–Au alloy and both 95Sn–5Ag and 1Sn–97.5Pb–1.5Ag solder alloys. He developed parabolic growth laws for both systems, and found that the Pb rich alloy exhibited considerably lower growth rates, especially at higher temperatures. At Sandia [67], preliminary work on a Pt–Au thick film alloy in contact with 63Sn–37Pb has indicated that a single layer intermetallic compound corresponding to $(Au,Pt,Pd)_1Sn_4$ forms, and the kinetics appear to be sub-parabolic over the temperature range 70° to 170°C. Figures 10 shows a set of x-ray elemental maps for a sample following a 120 h at 140°C anneal. Note that in addition to the planar layer of $(Au,Pt,Pd)_1Sn_4$ that "fingers" of intermetallic compound apparently extend down into the layer of unreacted thick film. These fingers are apparently due to the porosity that exists in the as-fired thick-film layer.

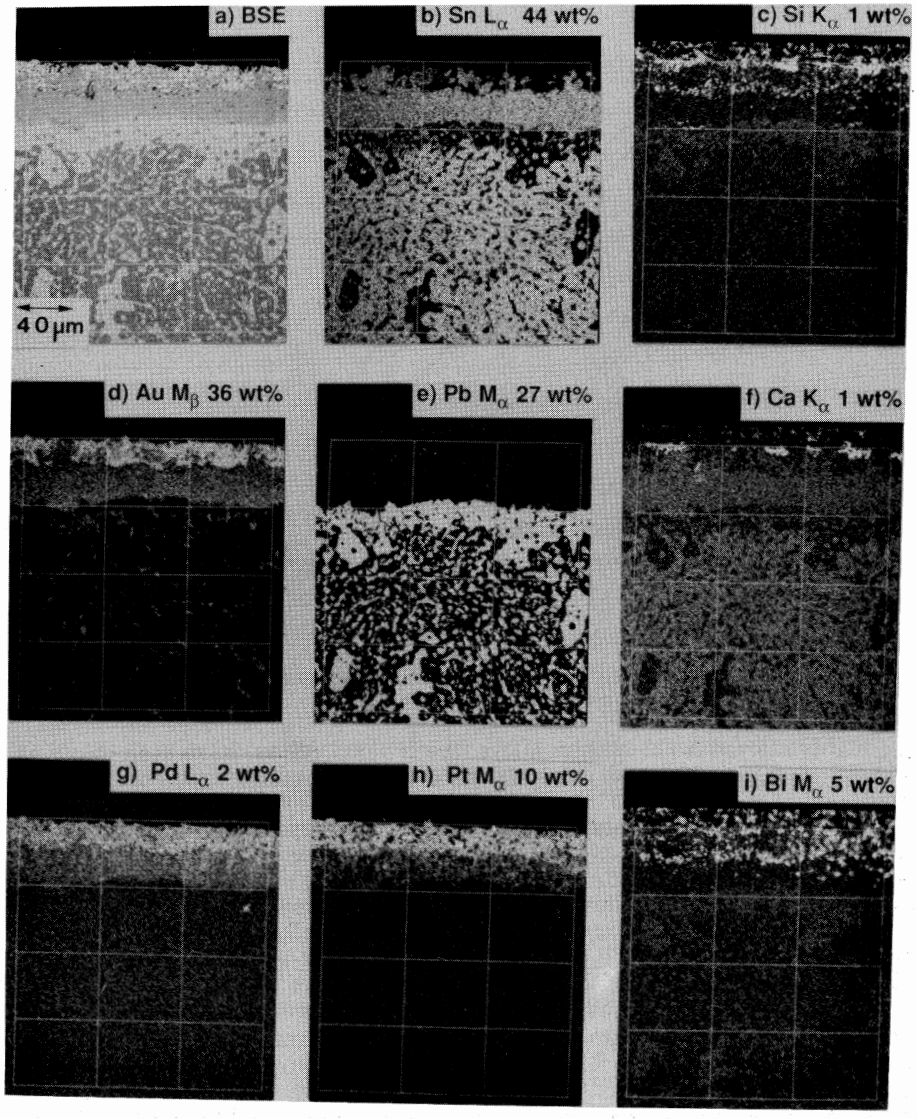

Figure 10 Backscattered electron image and wavelength dispersive elemental maps showing a thick-film Pt–Pd–Au/63Sn–63Sn–37Pb sampled aged for 120 h at 140°C. The thick film was printed and fired on a 96% alumina substrate [67].

Cu and Cu Base Alloys

There has been, in general, more intermetallic growth studies carried out on Cu and Cu alloys than any other base metal. A summary of these various studies is shown in Table 4 [24, 25,60, 68–78]. Table 4 indicates that the majority of the work has concentrated on the growth of intermetallics on Cu and its alloys in contact with Sn and Sn–Pb solder alloys. There are, however, published results for the system Cu and Cu alloys in contact with other solders (50Sn–50In [24, 25], 95Sn–5Ag [68, 76], 95Sn–5Sb [76] and 10Sn–88Pb–2Ag [76]). In general, the solid-state growth kinetics of Cu and Cu alloys in contact with various solders are fairly sluggish; either parabolic or subparabolic growth kinetics are usually observed for these systems. The only notable exception to this statement is the system Cu/50Sn–50In [24], where linear growth kinetics are observed. As a whole, the growth kinetics for Cu and Cu alloys in contact with solder alloys are much more sluggish than is the case for Au and Au alloys.

Table 4. Chronological summary of intermetallic growth studies: solders on Cu and Cu alloy substrates. All compositions shown are in wt.%. Samples were prepared by solder dipping unless otherwise indicated.

Reference(s)	Solder Alloy(s)	Substrate(s)	Comments
68	Sn, 97.5Sn-2.5Sb, 95Sn-5Ag and 60Sn-40Pb.	Cu	Samples annealed up to 32 dy at 100° to 200°C. Data plotted as total thickness versus log time.
69	Sn (diffusion couple)	Cu	Bulk Cu-Sn diffusion couples annealed up to 38 dy at 190° to 220°C. Motion of Mo markers indicated that Sn is the dominant diffusing species. Data plotted as thickness versus $t^{1/2}$.
60, 70	Sn, 70Sn-30Pb, 60Sn-40Pb, 30Sn-70Pb and 10Sn-90Pb (alloys plated onto substrates)	Cu 70Cu-30Zn	Long-term growth study. Samples annealed up to 365 days at RT to 170°C. Data plotted as total thickness versus $t^{1/2}$. Parabolic relations for growth of Cu_3Sn and Cu_6Sn_5 are presented [60].

71	45Sn-55Pb, 50Sn-50Pb, 55Sn-45Pb, 60Sn-40Pb, 65Sn-35Pb and 70Sn-30Pb	Cu	Short-term (100 h) anneals at 75° to 150°C were compared to the as-plated condition; parabolic kinetics were assumed. Results indicate that activation energy for growth of Cu_3Sn> Cu_3Sn +Cu_6Sn_5> Cu_6Sn_5. The three activation energies converge at lower wt.% Sn.
72	Sn, 60Sn-40Pb	Cu, C110, C194, C260, C706, C710, C713, C715, C725 and C752.*	Cu-20Ni superior to ETP Cu (C110) and α-brass (C260) in accelerated shelf life solderability tests up to 100 h at 150°C. In binary Cu-Ni alloys with plated Sn, up to 12% Ni accelerates intermetallic growth, while >20% Ni decreases the intermetallic growth rate.
73	Sn, 63Sn-37Pb, 30Sn-70Pb , 10Sn-90Pb, and 5Sn-95Pb	Cu	Micrographs showing intermetallic formation after 1000 h at 160°C. 10Sn-90Pb and 5Sn-95Pb alloys were observed to form Cu_3Sn only, while all others formed both Cu_3Sn and Cu_3Sn_5.
74	Sn, 60Sn-40Pb.	Cu	For 60Sn-40Pb alloy, activation energy for growth of Cu_3Sn and Cu_6Sn_5 were measured on both polycrystal and single crystal Cu substrates. Activation energy for growth of Cu_3Sn is ~2.5x that of Cu_6Sn_5 growth for both Sn and 60Sn-40Pb. Parabolic growth observed up to 600 h, and thickness of Cu_3Sn always less than thickness of Cu_6Sn_5.

24	50Sn-50In	Cu	Anneals performed at 70 to 110°C for up to 300 h, data were assumed to follow linear growth kinetics. Ternary compounds Cu_2In_3Sn and $Cu_2(In, Sn)$ were observed after aging using electron microprobe linescans.
75	60Sn-40Pb (plated onto substrates)	Cu phosphor bronze, Cu-15Ni-8Sn spinodal alloy.	Anneals performed from 80° to 135°C for up to 60 dy. Cu phosphor bronze alloy exhibits intermetallic growth similar to pure Cu, with formation of both Cu_3Sn and Cu_6Sn_5 observed. Only Cu_6Sn_5, along with a Ni-rich layer below it, was observed in aged samples of the Cu-15Ni-8Sn spinodal alloy.
76	Sn, 95Sn-5Sb, 95Sn-5Ag, 60Sn-40Pb, 30Sn-70Pb, 10Sn-90Pb, 10Sn-88Pb-2Ag, and 5Sn-95Pb.	Cu, C510, C172, C725, C727, C729, Cu-6Ni-4Sn, Cu-21Ni-5Sn, and Cu-23 Ni-5Co-8Sn.	Growth of intermetallics investigated from to 250°C for up to 167 days. Both Cu and C510 (Cu-5Sn-0.2P) form both Cu_3Sn and Cu_6Sn_5, while Cu-Ni-Sn and Cu-Ni-Co-Sn alloys form $(Cu, Ni)_6Sn_5$ only. Parabolic kinetics observed for all solder-alloy combinations studied. For 95Sn-5Sb, 95Sn-5Ag and 60Sn-40Pb, intermetallic growth rate peaks at 6 to 9 wt.% Ni in substrate alloy. Lowest intermetallic growth rates were observed with three Pb-rich solders.

77	Sn, 95Sn-5Pb, 74Sn-26Pb, 56Sn-44Pb, 30Sn-70Pb, and 10Sn-90Pb (plated onto substrate)	Cu	Short time anneals up to 14 dy at 75° to 175°C, 0.6 mm Cu wire with solder plate up to 22 μm thick. The 56Sn-44Pb exhibit highest value of activation energy for growth, assuming parabolic growth kinetics. Pb-rich layer does not act as a diffusion barrier for Cu-Sn intermetallic growth. Pb-rich alloys exhibited poorest solderability after accelerated aging at 110° to 175°C for up to 14 dy; apparently due to more stable oxides formed in the Pb-rich versus the Sn-rich alloys.

* Copper Development Association designations for Cu alloys. Consult *CDA Standards Handbook -Volume 2: Wrought Products* (Copper Development Association, Greenwich, CT) for exact compositions.

The case of pure Cu in contact with Sn and either 60Sn–Pb or 63Sn–Pb solder alloys is discussed first. In both cases, two intermetallic phases are observed as a result of long–term aging in these systems: Cu_6Sn_5 forms adjacent to the solder alloy, followed by Cu_3Sn adjacent to the Cu substrate. While it is possible that both intermetallics are present in the as–soldered condition (if time above melting point of the solder is long enough), the Cu_6Sn_5 is always observed in optical metallographic cross sections in the as-soldered condition. The Cu_3Sn phase is clearly resolved using optical metallography following a short annealing time (3 to 4 days) at 170°C. This is illustrated in Figure 7 where the Cu_3Sn phase is clearly resolved after 10 days at 170°C.

Numerous investigations [60, 68–74, 76, 77] have generated data on the solid state growth of the Cu–Sn intermetallics at temperatures less than the melting point of eutectic Pb–Sn solder (183°C). In most of these studies, the total intermetallic layer thickness is usually reported as a function of time at temperature, as opposed to measurements of the discrete thicknesses of the two Cu–Sn intermetallic phases. There are a few references where this has been done [42,71, 74], however, the data in these references usually only cover either isolated temperatures or relatively short ranges in time at aging temperature.

In terms of range of time and temperature,the most comprehensive investigation of intermetallic growth kinetics for samples of Cu/Sn and Cu/60Sn–40Pb was conducted during the early 1970's by MacKay and coworkers at the International Tin Research Institute (ITRI) [60, 70]. The majority of the ITRI data were generated on specimens consisting of electroplated layers of either Sn or 60Sn–40Pb on annealed wrought Cu substrates, followed by aging

treatments in air furnaces at temperatures between 70° and 170°C for times as long as 1 yr. A limited amount of work was also performed on Cu substrates that were hot dipped in 60Sn–40Pb solder; good agreement in growth kinetics for the two types of 60Sn–40Pb was indicated [60]. The resulting total intermetallic layer thicknesses for Cu/Sn and Cu/60Sn–40Pb(electroplated) as a function of time and temperature are plotted in Figure 11 and 12, respectively. In these Figures, the ITRI data has been plotted on log-log coordinates to emphasize the fact that the long-term growth kinetics for the combined growth of Cu_3Sn and Cu_6Sn_5 do not conform to a parabolic expression.

A least squares analysis was performed [61] on the data sets shown in both Figures 11 and 12 using Equation 3, with $x_0=0$ since the ITRI samples were plated as opposed to solder dipped. An excellent correlation with Equation 3 was obtained for the ITRI data, as is shown in Table 5. Note that the coefficient of determination r^2 for both of these data sets are greater than 0.96, suggesting that Equation 3 is an appropriate empirical expression to use to describe the intermetallic growth process. Note also that the time exponent n was determined to have values of 0.35 and 0.37 for the respective cases of Cu/Sn and Cu/60Sn–40Pb. These values of n are significantly less than the value of 1/2, which would apply if a parabolic growth law were an appropriate description of the overall intermetallic growth process. The previously mentioned (empirically determined) time exponents cannot be easily rationalized with a specific phenomenological layer growth mechanism, but they are useful for estimating the long-term growth of both layers. Comparisons of the results of the regression analysis with the data for both Cu/Sn and Cu/60Sn–40Pb are shown in Figures 11 and 12, respectively.

Using the correlations for intermetallic growth in the Cu/Sn and Cu/60Sn–40Pb systems shown in Table 5, long-term growth predictions [61] indicate that the total intermetallic thickness is greater for Cu/Sn than Cu/60Sn–40Pb at 60° to 100°C, and are approximately equal at 120°C; however, the total thickness at 140°C is expected to be larger for the case of Cu/60Sn–40Pb than for Cu/Sn. This is primarily a result of the apparent activation energy for intermetallic growth being slightly larger for 60Sn–40Pb than for pure Sn, hence a crossover in total thickness is encountered at 140°C and above. This crossover in growth rate was also observed by Unsworth and MacKay [70] at 135°C, and at 110°C by Yiyu et al. [77]. This result suggests that the Pb-rich layer that accumulates adjacent to the intermetallic (Figure 7b) in the case of either Cu/63Sn–37Pb or Cu/60Sn–40Pb is not an effective diffusion barrier at high temperatures, but may play some role in slowing intermetallic growth at the lower temperatures.

It is has been shown that the individual growth rates of Cu_3Sn and Cu_6Sn_5 could be each described by a parabolic growth law [74]. However, the growth rate of Cu_3Sn is apparently very sluggish, and was not determined below 125°C. The activation energy for the growth of Cu_3Sn is observed to be about twice that of Cu_6Sn_5, and the absolute growth rate of Cu_3Sn is always lower than that of the Cu_6Sn_5 over the temperature range investigated 90° to 170°C [74]. The fact that Cu_3Sn forms later suggests that Sn is the more mobile diffusing species. Onishi and Fujibuchi [69] observed that the net motion of diffusion markers in Cu–Sn couples at 190° to 220°C was toward the Sn side, also suggesting more rapid motion of Sn relative to Cu. This is consistent with what one would intuitively expect, since the melting point of Sn is so much lower than for Cu. The

formation of voids in the Cu–Sn alloy system are also a potential source of concern. If a large area of Cu were in contact with a small amount of Sn bearing solder, Kirkendall voids may form in the solder. The reduced effective cross-sectional area of the solder may be mechanically weakened and the mechanical properties of the solder joint compromised.

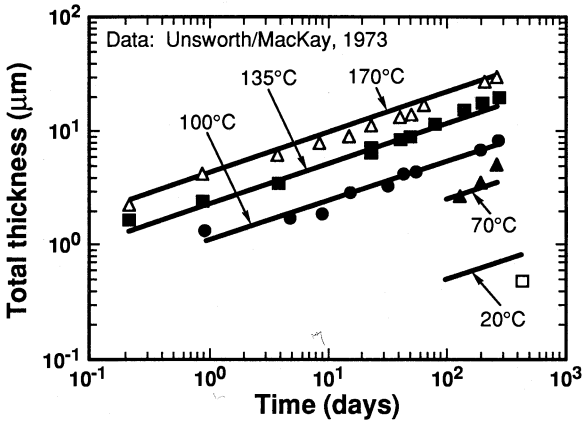

Figure 11 Long-term intermetallic growth kinetics for Sn plated on Cu [70]. The lines drawn for each temperature are the results of regression analysis [61] performed using Equation 3. The fit coefficients are listed in Table 5.

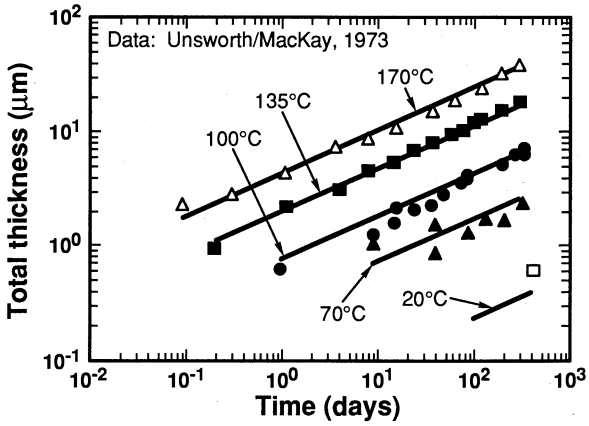

Figure 12 Long-term intermetallic growth kinetics for 60Sn–40Pb alloy plated on Cu [70]. The lines drawn for each temperature are the results of regression analysis [61] performed using Equation 3. The fit coefficients are listed in Table 5.

Table 5. Summary of regression analysis results on various substrate–solder combinations, using Equation 3. Note that x_0=0 for all of these data sets since the samples had either Sn or solder alloy plated onto the substrate.

System	# Points	T Range (°C)	A	Q (kcal/mol)	n	r^2
Sn plated on wrought Cu [60, 70]	35	20 to 170	7.18E3	6.523	0.347	0.968
60Sn-40Pb plated on wrought Cu [60, 70]	46	20 to 170	3.56E4	7.941	0.372	0.975
60Sn-40Pb plated on Phosphor Bronze [75]	12	80 to 135	8.63E3	6.206	0.273	0.942
60Sn-40Pb plated on Cu-Ni-Sn spinodal alloy [75]	10	80 to 135	2.15E3	6.179	0.192	0.775
Sn plated on Ag [60]	41	20 to 170	8.62E3	6.762	0.416	0.953

A significant amount of work has also been performed on Cu-based alloys, and these suggest that many Cu alloy substrates have significantly slower growth kinetics than pure Cu. LeFevre and Barczykowski [75] examined the growth of Cu–Sn intermetallics resulting from the plating of 60Sn–40Pb solder on both a phosphor bronze (nominal composition: Cu–5%Sn–0.2%P) and a Cu–15%Ni–8%Sn spinodal alloy. The plated specimens were aged at temperatures between 80° to 135°C for times up to two months. The total intermetallic thickness plotted as a function of the square root of time. The two data sets were fit to Equation 3, and the results are shown in Table 5.

Long–term intermetallic growth predictions [61] indicate little difference between the behavior of pure Cu versus phosphor bronze when in contact with 60Sn–40Pb alloy. However, the long term (30 to 40 yr at 60° to 140°C) growth predictions for Cu–15Ni–8Sn/60Sn–40Pb systems show results that are roughly an order of magnitude lower than the Phosphor Bronze/60Sn–40Pb stackup. Note

that the time exponent for the Cu–15Ni–8Sn/60Sn–40Pb stackup is significantly lower than all the other data sets shown in Table 5. A Ni-rich layer was observed close to the Cu_6Sn_5 layers, with no Cu_3Sn formation apparent in specimens of Cu–15Ni–8Sn/60Sn–40Pb aged at 80° to 135°C [75]. However, the work of Ohriner [76] indicates that although the growth rate of Cu–15Ni– 8Sn/60Sn–40Pb is less than that of Cu/60Sn–40Pb at 140°C, this is reversed at 175°C. Based on the apparent activation energy for Cu–15Ni–8Sn/60Sn–40Pb shown in Table 5, the results of Ohriner's work suggests that a different growth mechanism dominates this system at 175°C. This change in growth mechanism for Cu–15Ni–8Sn alloy is consistent with the results presented by Ohriner [76] for a variety of other solder alloys in contact with Cu–15Ni–8Sn.

Data for other Cu alloys suggest that alloying of Cu is a viable approach to minimize the solid state growth of intermetallics. For example, the intermetallic growth of α-brass (70Cu–30Zn) in contact with plated Sn exhibits a time exponent of 0.295 at 170°C, using the data of Unsworth and MacKay [70]. Figure 13 compares the 170°C growth kinetics for α-brass and Cu. For the case of the 95Sn–5Sb solder alloy, the Cu–23Ni–8Sn–5Co alloy [57] was found to have a slower intermetallic growth rate than pure Cu at 150°, 175°, and 200°C.

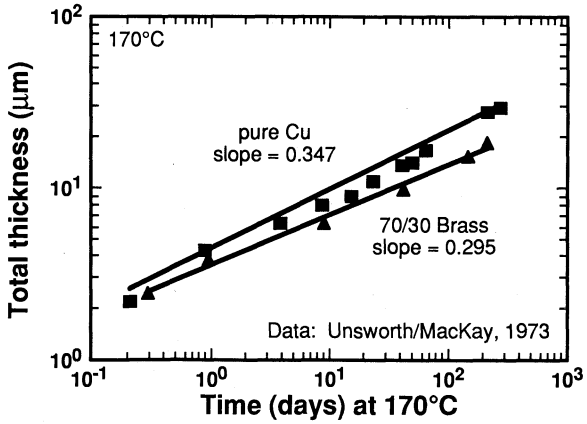

Figure 13 Long-term intermetallic growth kinetics at 170° for Sn plated on Cu and 70Cu–30Zn α brass alloy [70]. The line shown for Cu is calculated from the regression analysis coefficients listed in Table 5 for the Cu/Sn system, while the line for the α brass was obtained from regression analysis for the 170°C data only using a temperature - independent form of Equation 3.

Results for Other Base Alloys

A summary of studies on solid state intermetallic growth for other base metal systems is shown in Table 6 [20, 60, 70, 78–82]. While many of the references in Table 6 actually deal with plated layers of various metals on Cu or Cu alloy substrates, about half of the references shown [20, 60, 70,82] have examined intermetallic growth on bulk substrates of other metals. The work of Haimovich [20], discussed previously, also indicates that the intermetallic growth rate for Ni/Sn is significantly lower than Cu/Sn at temperatures less than 100°C, and the two systems have roughly equal growth rates at 150°C and above. This data

would help explain the interesting temperature dependence for the system Cu–15Ni–8Sn/60Sn–40Pb discussed previously.

Table 6. Chronological summary of intermetallic growth studies: solders on substrates other than Au and Cu alloys. All compositions shown are in wt.%. Samples were prepared by solder dipping unless otherwise indicated.

Reference(s)	Solder Alloy(s)	Substrate(s)	Comments
60, 70	Sn, 70Sn-30Pb, 60Sn-40Pb, 30Sn-70Pb and 10Sn-90Pb (alloys plated onto substrates).	Ni, Ag	Long-term growth study. Samples annealed up to 4 yr for Ag/Sn included. Ag observed to form only Ag_3Sn intermetallic. Highest activation energy for growth on Ag substrate observed with 60Sn-40Pb alloy. Ni observed to form both an inner layer of Ni_3Sn_4 and a Sn rich, acicular phase (wt. % corresponds to $NiSn_3$).
78	Sn (plated)	Ni-Sn, Pb, Ag, Ni, Co, Fe, Ni-Fe. (plated barrier layers on Cu and α-brass substrates)	All diffusion barrier metals were 5 μm thick except for Ag, which was 1 μm with 25-μm plated Sn. Results shown both for thickness of reaction layer of diffusion barrier with Sn, as well as reaction layers between either Cu-Sn and α-brass with Sn at 170°C. In general, Fe found to be best barrier layer, totally preventing passage of Sn. Ni, Ni-Fe and Ni-Sn also appear to be good diffusion barriers for Sn diffusion on both Cu and α-brass. Fe also had lowest rate of reaction with Sn.

79	Sn, 10Sn-90Pb, and Pb	60Ag-20Au-20Pd and 69Ag-31Au (fired from pastes)	Examination of role of Pd in intermetallic formation using diffusion couples under both solder processing and aging conditions. In contact with liquid alloys, Pd depleted regions observed near surface of 60Ag-20Au-20Pd alloy when in contact with 10Sn-90Pb alloy. Pure Pb reacts with Pd in 60-20-20 alloy to form Pb_2Pd reaction layer at 225°C. No interaction observed in solid-state couples between Pb and 69Ag-31Au after annealing at 200°C for up to 1000 h
80	Sn	Fe (plated barrier on Cu and α-brass)	Effect of thickness on performance of Fe diffusion barrier discussed. A 3-μm layer of Fe prevents Sn penetration to both Cu and α-brass after 500 days at 170°C.
81	60Sn-40Pb	Ni (plated onto phospor bronze clips)	A-1 μm Ni layer is effective in improving pull strength of terminal connections due to reduction of Cu-Sn intermetallic growth. Samples aged at temperatures 25-170°C for up to 10,000 h.
20	Sn, 90Sn-10Pb, 60Sn-40Pb	Ni	Intermetallic growth rate for Ni in contact with Sn is lower than Cu at temperatures <140°C. Aged Ni/Sn and Ni/90Sn-10Pb samples exhibit degraded solderability due to growth of acicular $NiSn_3$ phase. The kinetics of thermal decomposition of metastable $NiSn_3$ phase are characterized using Avrami-Johnson-Mehl equation.

82	60Sn-40Pb 50In-50Pb	Paliney 7™ alloy (Pd-Ag-Cu-Au-Pt-Zn)	Intermetallic growth kinetics characterized at 80°, 110° and 140°C for up to 1000 h Paliney 7 exhibits close to parabolic growth kinetics when in contact with 60Sn-40Pb, and approximately inear kinetics with 50In-50Pb alloy. The complex intermetallic layer formed for Paliney 7/60Sn-40Pb samples appears have majority phase of Pd-Sn and Pd-Pt-Sn intermetallics, along with Ag_3Sn and Cu_3Sn islands distributed through the intermetallic layer.

Ag/Sn is another system that was well characterized by the ITRI researchers [60, 70]. As was the case for Cu alloys, Ag samples were prepared with plated Sn, and annealed for long times at temperatures between 20° and 170°C. The authors indicated that the only reaction phase observed was Ag_3Sn; it is interesting to note [21] that this implies that the Ag-rich ζ phase, which extends from 11.8 to 18 wt.% Sn, is not observed. The ITRI data [60] has been replotted on double logarithmic coordinates in Figure 14. As in the case of Cu/Sn, the kinetic exponent 0.42 is observed to be slower than the parabolic exponent of 1/2. Note that the apparent activation energy for Ag/Sn is only slightly higher than is observed for Cu/Sn (Table 5).

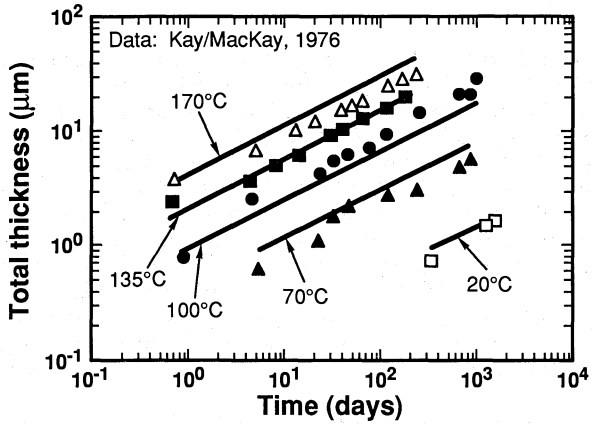

Figure 14 Long-term intermetallic growth kinetics for plated Sn on Ag [60]. The lines drawn for each temperature are the results of regression analysis [61] performed using Equation 3. Table 5 lists the fit coefficients.

Growth kinetics for the precious metal glassing alloy Paliney 7™ (Pd–Ag–Cu–Au–Pt–Zn alloy) in contact with 63Sn–37Pb and 50In–50Pb solder alloys have also been determined [82]. The time exponent for Paliney 7/63Sn–37Pb was found to be 0.46, which suggests approximately parabolic kinetics, while linear kinetics were observed for Paliney 7/50In–50Pb. The differences in growth kinetics, along with the poor wetting behavior of 50In–50Pb on Paliney 7, indicated that 63Sn–37Pb is the preferred alloy to use for soldering to Paliney 7.

The other references shown in Table 6 deal with the use of diffusion barriers to prevent the growth of Cu–Sn intermetallics. Kay and MacKay [78] performed a rather exhaustive study of various diffusion barriers (5 μm thickness) on Cu in contact with electroplated Sn. Based on long-term aging tests at 170°C, they identified Fe as the most promising diffusion barrier for this system. Using the 5-μm thick Fe diffusion barrier, formation of $FeSn_2$ was observed, but at a very slow rate: at the end of 400 days at 170°C, pure Fe was still observed and no Cu–Sn intermetallics were formed. Warwick and Muckett [80] investigated thinner plated layers of Fe under the same conditions, and found that a 3 μm plated Fe layer was an adequate diffusion barrier, while thinner layers of Fe were not. Ni [78, 80] was found to fully react with the Sn by the end of the long term aging (170°C, 400 days), however, it was significantly slower than other pure metal diffusion barriers that were examined (Co, Ag, and Pb). Based on these results, it would appear that a reasonable diffusion barrier system for Cu that would combine low intermetallic growth kinetics along with good shelf life for solderability would be Fe with an outer layer of Ni. This diffusion barrier system could be pretinned with 63Sn–37Pb and one could thereby avoid the storage problems associated with reflowed Sn on Ni [20].

Introduction to Intermetallic Phases in Soldering

EXPERIMENTAL MEASUREMENT OF INTERMETALLIC LAYER THICKNESS

Intermetallic compound layer thickness is measured by using traditional metallographic techniques, including optical metallography, scanning electron microscopy (SEM) and analytical transmission electron microscopy (TEM). Optical metallography is typically the preferred method because of its simplicity. SEM is often used when intermetallic layer thicknesses of less than 1 μm are being measured or if it is not possible to distinguish two phases from each other under the optical microscope due to lack of relative contrast. The SEM or electron probe microanalyzer (EPMA) can also be used to collect elemental maps using characteristic x-rays or to measure the composition and thereby identify the intermetallic phases. The TEM is used only to study very thin intermetallic layers (< 0.1 μm). Such thin layers are likely to form very early in a reaction, or they can possibly be present during the entire growth process if diffusional fluxes are such that the intermetallic layers simply do not grow very thick.

The metallographic preparation of solder joints is very much an art. The solders are typically very soft, while the intermetallic compounds tend to be very hard. The substrate may be either hard or soft. For example, a Cu–Be substrate will be very hard while a pure Au substrate will be very soft. This hardness variation can be further exacerbated if the joint was formed on a thick- or thin-film metallization layer on a ceramic substrate. This large range in hardness across

the joint makes polishing very difficult. Great care must be taken to prevent the various constituents from smearing across one another, especially if the analytical objective will be compositional analysis with the SEM or EPMA. Once a suitable polish is obtained, the appropriate etching procedure is required to generate optical contrast between the various layers. Often a trial and error procedure, coupled with SEM examination, will be required to develop a suitable etching procedure. It is not appropriate to describe the wide range of metallographic procedures here and the reader is referred to the literature [83].

In some cases, it is not possible to use optical metallography because sufficient contrast between the phases was not generated by the etching procedure or because the layer thicknesses of interest are below the resolution limit for optical metallography (~ 0.5 μm). In such cases, the SEM should be used. Specimens examined in the SEM or EPMA are often polished, but not etched, to avoid the creation of artifacts. If the specimen has been properly polished there will be very little surface relief. As such, phase contrast will not be carried by secondary electrons and little contrast will be observed in the normal SEM imaging mode. However, there is often a large average atomic number difference between the substrate and the solder and intermetallic layers. Such atomic number contrast is readily observed with backscattered electrons (BSE). If further information is required beyond what can be observed in the BSE mode, it will be necessary to use elemental x-ray mapping. For optimum results, the mapping should be done with the wavelength dispersive spectrometer (WDS) rather than the energy dispersive spectrometer (EDS). The signal from the WDS has a much larger signal to noise ratio than the EDS and will generate far more contrast in the map. Usually only EPMAs have diffracting crystals sensitive to the proper wavelength to collect good maps. Figure 15 illustrates a typical sequence of images. The specimen is a Au thick-film metallization on alumina in contact with Pb–In solder. The Au has reacted with the solder to form the intermetallic compound ($AuIn_2$) while aged at 130°C for 200 h. Figure 15 shows the BSE image. The Au is the brightest, having the highest atomic number and hence the greatest yield of BSE. The intermetallic compound (Pb free) is somewhat darker. The solder is intermediate in brightness due to the Pb contact. The alumina is of such a low atomic number that it appears completely dark. Figures 16 and 17 show the corresponding elemental x-ray maps for Au and In. For further details on image formation, signal generation and mapping in the SEM and EPMA, the reader is referred to the basic literature [84].

To examine very fine intermetallic layers (< 0.1 μm) it may be necessary to use the TEM. TEM examination of solder joints is rarely done and therefore references in the literature are extremely rare. The TEM examination of a solder joint is actually somewhat routine, but the preparation of specimens is perhaps the most difficult in the entire realm of TEM in materials science. The authors do not know of any general references on sample preparation of solder joints for the TEM. There are, however, a few references to specific problems [85]. It is suggested that the soldering metallurgist work closely with the staff in the TEM laboratory if such a problem is encountered. For more general information on the TEM, the basic literature is again suggested [86, 87].

Once suitable micrographs (such as optical, SEM, and x-ray) have been obtained it is necessary to measure the layer thicknesses. Since the interfaces are often somewhat nonplanar, the determination of the layer thicknesses is often a tedious task. Care must be taken to insure that the measurements are not biased

by the individual making them. The recommended procedure is to take perhaps five micrographs along the joint at a magnification in which measurements can be readily made. Each micrograph should then have a grid laid across it and measurements made systematically along the length of the joint. If the metallographer makes the measurements by personal choice, the data will be biased. Such a measurement procedure yields an accurate average thickness measurement, but may produce an artificially large standard deviation. One possible procedure to reduce the scatter is to *mass balance* the interface, as shown in Figure 18. A reference line is drawn through the interface so that the areas included on both sides of the interface are equal. Such a procedure should be performed on up to 30 micrographs. The result should be an average thickness essentially identical to that obtained with the first procedure, but with a more realistic standard deviation.

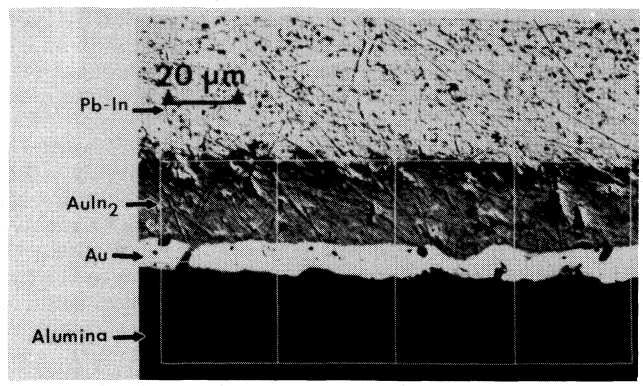

Figure 15 Backscattered electron image of Pb–In solder in contact with an Au thick film. Aged at 130°C for 200 h. Intermetallic phase is $AuIn_2$.

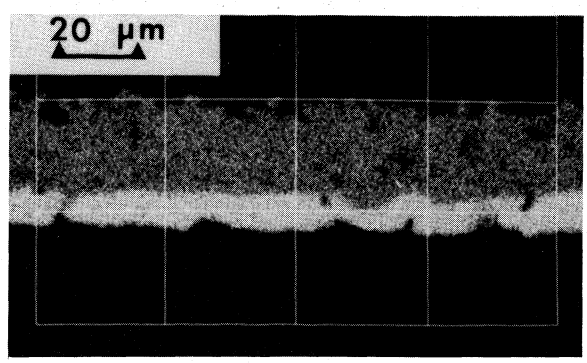

Figure 16 Elemental x-ray Au map of specimen shown in Figure 15. Collected by wavelength dispersive spectrometer in an electron probe microanalyzer.

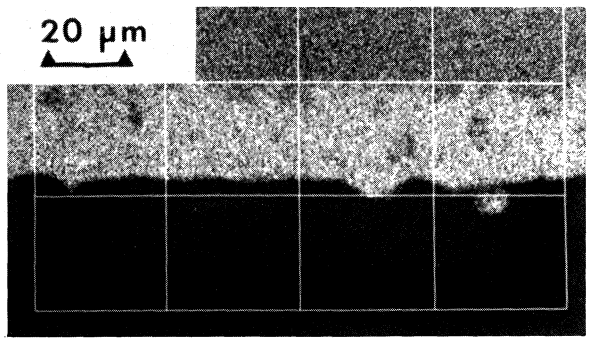

Figure 17 Elemental x-ray In map of specimen shown in Figure 15. Collected by wavelength dispersive spectrometer in an electron probe microanalyzer.

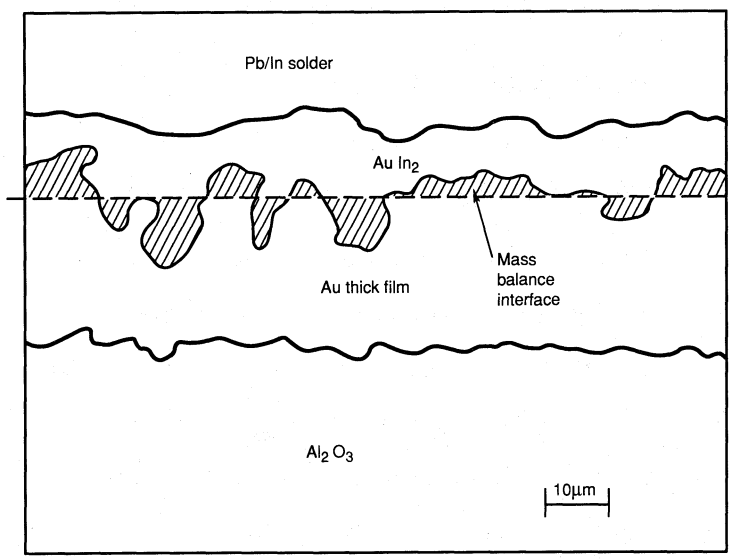

Figure 18 Example of procedure to smooth an interface using the mass balance at the interface technique.

PROPERTIES OF INTERMETALLIC PHASES

There is a limited amount of data on the microhardness of various intermetallic compounds that result from the reaction of solders with base metals, and is assembled in Table 7 [49, 53, 95–97]. It is important to note that except for the data of Bester [53], which was from a bulk Au–Sn alloy, all of the data shown in Table 7 were generated on relatively thin layers from solder–substrate samples. As such, there may be problems with the strict validity of some of the data; relatively low load levels were used and the indents may have spanned the entire

layer thickness. Despite these caveats, it is apparent that the microhardness of both Cu–Sn intermetallics is apparently much higher than either of the Au–Sn or Au–In intermetallics shown in Table 7. One reason for this, at least in the case of the data shown for $AuIn_2$, is that layers of $AuIn_2$ resulting from the growth of Au substrates with 50Pb–50In solder alloy often contain entrapped Pb phase, which undoubtedly helps to reduce the brittleness of these layers [49]. It is not clear why the microhardness value for $AuSn_2$ reported in Table VII should be so low, insofar as $AuSn_2$ and $AuSn_4$ are thought to be extremely brittle intermetallics [53]. It is apparent that microhardness as well as other mechanical property data should be generated on bulk samples of these intermetallic compounds. Macroscopic mechanical properties of the important intermetallic compounds have not yet been measured, although efforts to make such measurements are underway at several laboratories.

Table 7. Summary of microhardness data for intermetallic compounds (IMC). Data for base metals are included where available from same investigation.

IMC	Ref	Microhardness - As Reported
Cu_3Sn	[90]	590 kg/mm^2 (indentor type/load not described)
Cu_3Sn	[89]	400 MHN (5-gm load, presumably with Vickers indentor)
Cu_3Sn	[88]	350 kg/mm^2 (Knoop indentor, load not described)
Cu_6Sn_5	[90]	630 kg/mm^2 (indentor type/load not described)
Cu_6Sn_5	[89]	550 MHN (5-gm load, presumably with Vickers indentor)
Cu_6Sn_5	[88]	450 kg/mm^2 (Knoop indentor, load not described)
Cu	[88]	95 kg/mm^2 (Knoop indentor, load not described)
$AuIn_2$	[89]	280 MHN (5-gm load, apparently with Vickers indentor)
$AuIn_2$	[49]	85 Knoop (10-gm load)
$AuSn_2$	[53]	100 DPH (presumably with 25-gm load)
Au	[49]	62 Knoop (10-gm load)

Phase Stability, Diffusion Paths and Multilayer Growth

The preceding sections treated the diffusion processes which occur between solders and substrates in a very simplistic manner. For example, all systems were treated as binaries and the kinetics analyzed were those for layer growth and not diffusion. Most solder-substrate problems are actually at least ternary systems and so an understanding of multicomponent thermodynamics is really required to understand the formation of intermetallic compounds in the solder joint. Furthermore, layer growth kinetic analyses for systems containing more than one intermetallic compound layer are strictly valid only over the temperature range in which they were made. The diffusional processes which control the growth of each layer may have vastly different activation energies. It is possible that the growth of one compound will dominate at the temperature range studied in the laboratory, while the growth of another compound will dominate at the actual service temperature. As a consequence, extrapolations of simple layer growth results to lower temperatures may be very inaccurate. The best way to approach this problem is to determine the diffusivities in each layer in the joint and then to solve the multilayer diffusion problem at the temperature of interest. This procedure will eliminate the extrapolation uncertainty. The only remaining uncertainty will then be a mechanism shift; for example, from volume diffusion control to interface reaction control.

This section gives the details of the thermodynamics of ternary systems and describes the diffusion controlled multilayer growth process. This approach is phenomenological (based on thermodynamics) rather than empirical. It is the most accurate method for modeling microstructural evolution in solder joints. However, its application is often limited by the unavailability of phase diagram and diffusion data.

THERMODYNAMIC CONSIDERATIONS

The reactions between solder alloys and substrate materials depend upon the thermodynamics and kinetics of a multi-component system. Since most solder alloys consist of more than two elemental components, a ternary (or higher order) system is involved even when the substrate is a pure metal. The first question that needs to be addressed is thermodynamic stability (the equilibrium phase diagram).

Figure 19 shows a hypothetical phase diagram of a ternary system, A–B–C, at constant temperature and pressure. It is assumed that both A and B, designated as α and α', have the same crystal structure and form a miscibility gap. The component C, designated as β, has a different crystal structure. The solubility of B(α') in C(β) is negligible, while that of C(β) in B(α') is significant. Due to the solubilities of A(α) and C(β) in B(α'), the single-phase field of α' exists in the ternary region. In the binary C–A, two intermediate phases, γ and δ, exist. Both of these phases are in equilibrium with α', as shown in Figure 19.

A large amount of thermodynamic stability information is contained in such a phase diagram. For instance, when an alloy α'(b) is in contact with an alloy α(a), no reaction occurs since these two alloys are in thermodynamic equilibrium. The same situation is also true when the alloy α'(b) is in contact with δ. Conversely, when the alloy α'(b) is in contact with pure A, there is a small amount of reaction

at the interface until a sufficient amount of time is allowed for B and C to dissolve in A and reach the composition α(a).

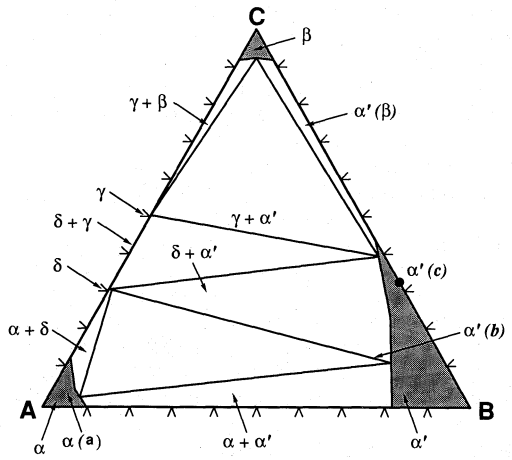

Figure 19 Isothermal section of a hypothetical ternary system A–B–C.

The following is a discussion of the thermodynamic stabilities of two couples taken from such a hypothetical ternary system: pure A/pure B and pure A/α'(c). Pure A and B are not in thermodynamic equilibrium because of their mutual solubility limits. The reaction will occur at the interfaces until the solubility limits are reached. The phase diagram of the binary A–B alone describes the equilibrium compositions at the interfaces, assuming local equilibrium at the interface. The situation for the second case, A/α'(c), is much more complex. Here A and α'(c) are not in thermodynamic equilibrium and a reaction occurs at the interfaces. The intermediate phase δ and the α'-phase with a different composition will form at the interfaces. However, the phase diagram does not describe how the phases are formed, even when planar interfaces prevail. The diffusion path must be known, as discussed in this section.

A phase diagram, as shown in Figure 19, is normally determined experimentally. Since solder–substrate interactions involve initial solid-liquid reactions, subsequent solidification reactions, and eventually solid-state aging reaction, it is necessary to have the phase diagram of A–B–C as a function temperature. Very few ternary phase diagrams are determined accurately even at two temperatures, much less over a wide range of temperatures. The most powerful way to establish the phase diagram of a ternary system over a wide range of temperature is the combined computational and experimental approach. This approach has been used extensively by Chang and coworkers at the University of Wisconsin [91–94] for a variety of multi-component systems. Currently, Chang and Bolcavage, in collaboration with Romig of Sandia National Laboratories, are studying ternary Cu–In–Pb, a system of technological interest for soldering in microelectronic devices [95]. Boettinger and Kattner [96] of NIST are currently studying the Cu–Pb–Sn system in a similar manner [96].

If the thermodynamic data, Gibbs energies of all the phases involved (α, β, γ, and δ) are known, it is possible to compute the diagram shown in Figure 19. Normally, the thermodynamic data for some of the binary solution phases and binary intermediate phases are known. The data for the ternary phases are rarely known. In practice, the available thermodynamic and phase equilibrium data for the three binaries are assessed first. This type of assessment requires a high level of understanding of solution thermodynamics and computational techniques, and yields a set of internally consistent thermodynamic values for all the binary phases involved. On the basis of the thermodynamic values for the binary phases and an appropriate extrapolation technique [97], thermodynamic values for the ternary phases are obtained. The calculated phase diagram is compared with experimental data if available. If data are not available, key experiments may be performed to verify the calculated diagram. If there are any discrepancies, the phase diagram data are used to optimize the ternary parameters introduced. These parameters are estimated using one of the extrapolation methods [97]. This type of analysis ultimately yields a set of parameters for all the phases involved for the ternary system. Once the parameters for the phases are known, it is possible to calculate not only the stable, but also metastable, phase diagrams as a function of temperature. This is undoubtedly the best approach in generating phase diagram information for technological applications.

For solution phases, the excess Gibbs energy of a phase such as that given in Figure 19 can be represented by the following equation:

$$\Delta^{xs}G^{\alpha}/RT = \frac{1}{2}\sum_{j=1}^{3}\sum_{i=1}^{3}\left[w_{ij}^{\alpha}\, x_i x_j + \left(w_{ij}^{\alpha} - w_{ji}^{\alpha}\right) x_i x_j^2 - 4\, v_{ij}^{\alpha}\, x_i^2\, x_j^2\right] + w_{123}^{\alpha} x_1\, x_2\, x_3 \qquad (4)$$

where $\Delta^{xs}G^{\alpha}/RT$ is the excess Gibbs energies of the alloy $\alpha(x_1, x_2)$; x_i, x_j are the atom fractions of the component elements, R is the gas constant and T is the absolute temperature, with the superscript xs meaning excess. The quantities w_{ij}^{α} and $v_{ij}^{\alpha} = v_{ij}^{\alpha}$ are the solution parameters of the binary phases and w_{123}^{α} is a ternary solution parameter. Values of w_{ij}^{α} and v_{ij}^{α} which are temperature dependent are obtained from an analysis of the binary data. Values of w_{123}^{α} can be estimated from one of the extrapolation techniques and may be optimized using ternary data when available. Occasionally, more than one ternary solution parameter is needed. The additional ternary interaction terms are added to Equation 4.

Equation 4 may be used to describe the data for all other solution phases such as the β and the liquid phases for A–B–C given in Figure 19. For γ and δ, they are taken to be line compounds.

To carry out the analysis as presented above, it is necessary to know the lattice stabilities of the component elements A, B and C. In other words, the Gibbs energy differences between the various crystal structures, such as between α and β, need to be known. The Gibbs energies of melting must also be known.

Interfacial Equilibrium

Virtually all modeling of diffusion controlled phase growth, including the growth of intermetallic compound layers in solder joints, makes use of the assumption of equilibrium at the phase interfaces. This assumption states that the interface, being crystallographically incoherent, has a composition defined by the appropriate two-phase tie-line end points from the equilibrium phase diagram. Figure 20 shows the schematic relationship between tie-line endpoint compositions and the composition of phase interfaces. In this example, two pure phases, α and γ, react to form intermediate phase β. In a more complex system, such as that formed by Au or Cu with a solder, multiple intermetallic compounds will form but the interfacial compositions will still be defined by the tie-line endpoints. While this assumption is widely used, it has on occasion been challenged, and it is important to consider the validity of this assumption before blindly applying it to intermetallic layer growth between substrates and solders. The topic of interfacial equilibrium in intermediate phase growth has recently been reviewed in detail by Romig [98].

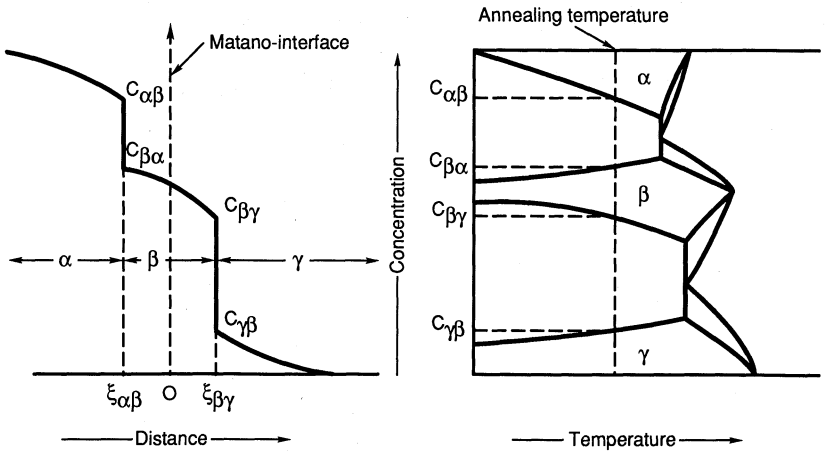

Figure 20 Relationship between interfacial composition and composition from tie-line endpoints from the phase diagram.

The assumption of local equilibrium at phase interfaces, or interfacial equilibrium, is often invoked during experimental studies of coexisting phase stability [99–103]. Since the assumption implies that the composition of the phases coexisting at the interface are those given by the equilibrium tie-line on the (incoherent) phase diagram, the contributions of such effects as curvature and stress are totally neglected. Much progress has been made over the past few decades in investigating the theoretical nature of interfacial equilibrium [104–111] However, experimental investigations of interfacial equilibrium are much rarer [112]. These recently reported experimental results all suggest that at the size scales of importance for intermetallic layer growth in solder joints, the interfaces are fully incoherent and the interfacial equilibrium assumption is valid.

Thermodynamics of Interfaces

The thermodynamics of phase interfaces play a major role in defining the equilibrium state that exists between two coexisting phases. This thermodynamic state defines the boundary condition for the diffusion equation (which describes the growth of the intermediate phase) as well as contributing to the driving force for growth. The condition of thermodynamic equilibrium can readily be illustrated on a free energy (Gibbs free energy, G) versus composition plot, as shown in Figure 21. The free energy curves for two coexisting phases (such as substrate and intermetallic phase) are shown. The equilibrium composition of the coexisting phases can be determined by the classical common tangent construction [113]. If the microstructure is still evolving (as evidenced by concentration gradients in the coexisting phases), then the construction in Figure 21 gives the interfacial composition. Curvature effects, strains and external fields (such as electrical) can perturb this equilibrium, as is also shown in Figure 21.

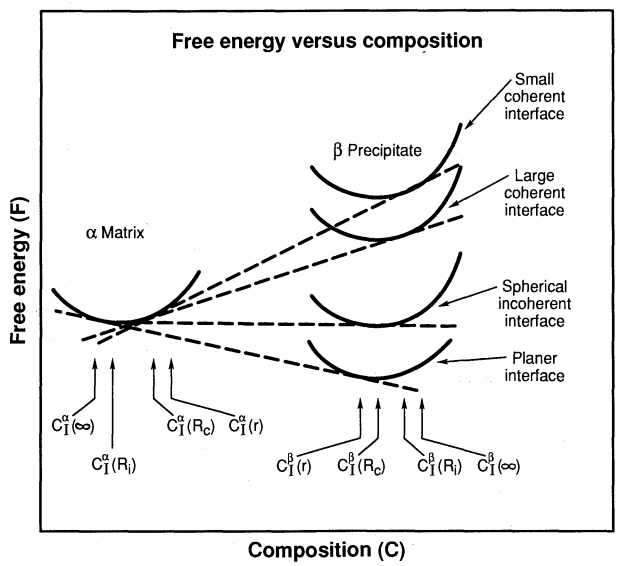

Figure 21 Free energy versus composition diagram illustrating how the nature of the precipitate-matrix interface influences phase equilibrium. The sub-I indicates interfacial composition. The sub-o indicates the matrix composition. The precipitate phase (intermetallic layer) is denoted by β and the matrix phase (substrate or solder) by α. The parenthetical ∞, R_i, R_C and r indicate composition for a planar incoherent interface, a curved incoherent interface, a curved coherent interface with a large radius curvature and a curved incoherent interface with a small radius of curvature.

Experimental Measurements of Interfacial Equilibrium

Interfacial phase equilibrium has been investigated in detail in several systems including Cu–Al [111], Fe–Ni and Fe–Ni–P [114–118] and U–Nb [119] by EPMA and analytical electron microscopy (AEM). In all cases, once the intermediate phase had grown to a size in which interfacial composition could be determined

(>50 nm), the interfacial compositions were those given by the incoherent phase diagram.

Interfacial Equilibrium in Solder Joints

Currently, all data reported in the literature concerning the growth of intermetallic layers in solder joints pertain to well-evolved microstructures in which the intermetallic layers are at least several tenths of a micrometer thick. At this spatial scale, the interfaces are fully incoherent and there are no coherency strains. Also, the curvature is very small and the interfacial equilibrium is not perturbed. If one is examining structures of this scale, the interface can be considered to be incoherent and one can assume that the interfacial compositions are those given by the phase diagram. However, one important caveat must be noted. As attempts are made to study intermetallic growth at very early stages, the effects of coherency strain and curvature may be important. It is possible that at some point in the near future, the issue of interfacial equilibrium in solder joints may need to be revisited.

KINETIC CONSIDERATIONS

Mechanisms for Intermetallic Phase Growth

The growth of intermetallic phases can be controlled by either volume diffusion through one of the phases or by interfacial reaction kinetics. If the growth is controlled by volume diffusion through one of the phases, the kinetics will be parabolic in time. If the growth is controlled by interfacial reaction kinetics, the kinetics will be linear width time. Examples of these two kinetic behaviors were given in the previous section.

In any reaction that produces an intermediate phase, diffusion must occur in all of the phases and reactions must occur at all of the interfaces. The final kinetic behavior exhibited by the system will be that of the rate limiting step. This is illustrated schematically in Figure 22. Note that since volume diffusion and interfacial reactions are thermally activated, their relative rates may change with temperature. Hence, the rate controlling step, and therefore the kinetics, may change with temperature. As such, it is extremely important to extrapolate kinetics outside of the temperature range in which they were measured with great caution. Furthermore, it is possible for kinetics to change even under isothermal conditions. For example, consider a case where a reaction is initially controlled by interfacial kinetics. This means diffusion has no difficulty in providing reactants to the interface. As the reaction proceeds, the distance over which diffusion must occur becomes longer. Eventually, diffusion may not be able to supply all of the reactant needed at the interface and the reaction will switch to diffusion control. Hence, a full understanding of the microstructural evolution process is needed before one can extrapolate kinetics with complete confidence.

Diffusion Paths: Volume Diffusion Control in Ternary Systems

Consideration of diffusion paths is important if the reaction at the interface is volume diffusion controlled in alloy systems with at least three components (i.e., Cu–Sn–In). It is the combination of thermodynamics and kinetics that determines which intermediate phases will form in the diffusion couple (such as

solder–substrate is a diffusion couple). Thermodynamics describes what will happen when equilibrium conditions are achieved, but does not describe what combinations of phases may form under actual conditions. For instance, it is not possible to determine what phases will form when α'(c) is in contact with pure A from the phase diagram given in Figure 19. While only one diffusion path is possible in a binary couple, this is not true for a ternary couple. When pure B is in contact with pure A, dissolution of B in A(α) and of A in B(α') will occur until the mutual solubilities are attained.

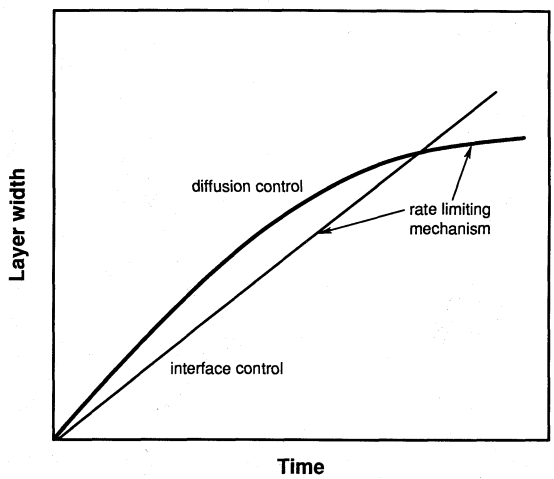

Figure 22 Comparison of interfacial and volume diffusion control. Rate limiting mechanism is shown.

Similarly, when C is in contact with A, δ and γ will form in addition to the attainment of the solubility limits of C in A(α) and of A in C(β). Conversely, when α'(c) is in contact with A, there is more than one possible diffusion path. Figures 23 shows two possible diffusion paths. In path I, the phase δ is in contact with α'(b) and α'(d) while in path II, d is in contact with α and α'(e). According to Kirkaldy and Brown [120], given a specific semi-infinite ternary diffusion couple, there is only one diffusion path at constant temperature and pressure. Recent experimental studies by Van Loo and coworkers [121–124] on oxide-metal systems, Leute [125] on pseudo-ternary compound-compound semiconductor systems, and by Chang and coworkers [126–134] on GaAs-metal systems yield results in accordance with this statement. Although it is possible in principle to calculate the diffusion path, given the current state of understanding of ternary systems of technological interest such as Cu–Pb–Sn and Cu–Pb–In, in practice it is impossible. Experiments must be performed to determine the diffusion paths of most ternary couples of current technological interest.

Interface Morphology

Up to this point, the interface morphology has not been discussed from the theoretical perspective. The interface is determined by the growth kinetics of the phases in a couple. Wagner [135] considered the morphological and kinetic

aspect of displacement reactions in the solid state. In a later paper [136], he established the criteria for the stability of a planar oxide-alloy interface during the oxidation when the oxygen is the predominant diffusing species. More recently Zhang [137] extended the Wagner formulation to the case when oxygen is the dominant diffusing species. Furthermore, he has applied the criteria to determine the interfacial oxide-alloy stability during the oxidation of (Pb–In) alloys. Chang and coworkers have used this concept to study the reactions in GaAs-metal couples [132, 133, 138, 140] and Rapp and coworkers [141–143] studied the reactions in oxide-metal and sulfide-metal couples.

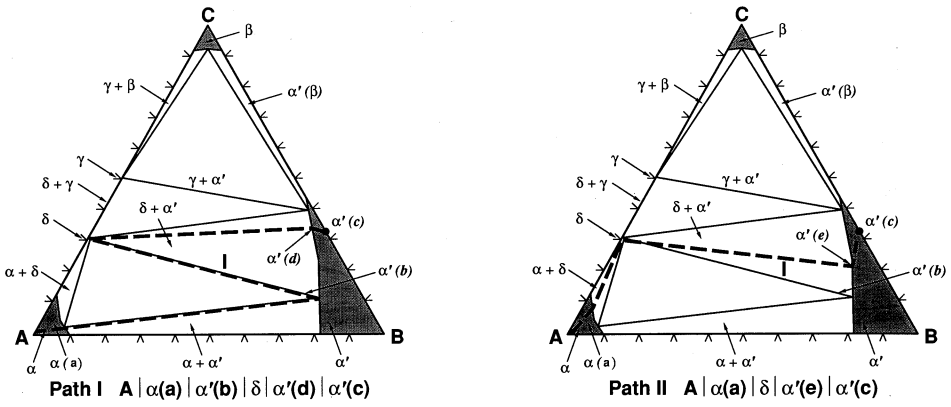

Figure 23 a) A possible diffusion path (Path I) for a semi-infinite couple of A/ α'(c). b) Another possible diffusion path (Path II) for a semi-infinite couple of A/ α'(c).

This concept will now be applied to a diffusion couple of A/α'(c) (Figure 19), with the diffusion path being path II, shown in Figure 23. The path is A/α/δ /α'(e) /α'(c); only one intermediate phase is formed between A and α'(c). Assuming that the initially predominant moving species is C, the growth front of δ would necessarily occur at the α/δ interface as shown in Figure 24. The growth of δ is controlled by the diffusion of C from the α'/δ interface through the phase δ. The flux of C arriving at position II exceeds that at position I, resulting in the formation of a planar α/δ interface. However, under other conditions, non-planar interfaces may prevail as have been discussed in the literature [136–143].

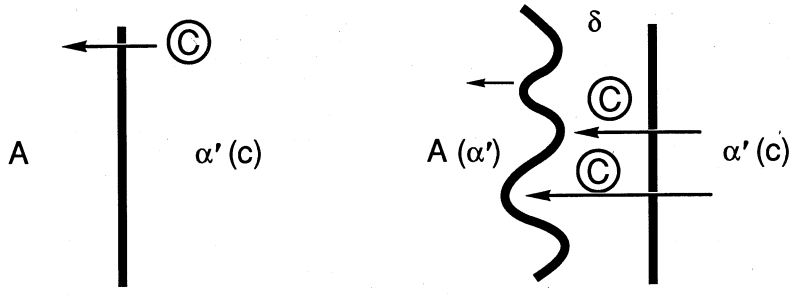

Figure 24 A possible interface morphology for a semi-infinite couple of A/ α'(c).

Phase Formation Sequence

The diffusion path of a ternary diffusion couple such as A/α'(c) represents the stable phase arrangement between the end phases, A and α'(c) for this couple. However, depending upon the types of phase equilibria and the relative mobilities of the component elements in the various phases, the phases formed initially, and even the phases formed subsequently, may not correspond to the stable phase arrangements. This phenomena has been well documented in several GaAs-metal systems [126,127,129,132,133]. In fact, for the GaAs-metal couples, knowing the phase equilibria of the ternary and the component diffusivities, Chang and coworkers have formulated general guidelines for forecasting the phase formation sequences [138–140].

The phase equilibria of certain ternary systems of relevance to soldering technology, such as Cu–Pb–In, are not known. It is practically impossible to say anything about the phase formation sequence when a solder alloy of Pb–In is in contact with a Cu substrate. However, in view of the overwhelming evidence for the formation of metastable equilibria in the GaAs-metal systems, the similar phenomena in solder systems of technological interest may be possible, and have been documented in the case of Ni/SnPb alloys [20]

Quantitative Layer Growth Analysis

Up to this point, only the qualitative arguments for the formation of phases in a ternary diffusion couple of A/α'(a), as shown in Figure 19, have been discussed. Now the basic quantitative formulation for the growth of phases formed in a bulk diffusion couple in terms of ternary diffusion theory is detailed.

A solution to the diffusion equation for the growth of a two-phase binary system was proposed by Wagner as given in Jost [144]. Subsequently, this solution was extended to three-phase binary systems by Castleman [145] and to n-phase binary systems by Kirkaldy [146] and Kidson [147]. Heckel and coworkers [148] and Metin, Inal and Romig [149], among others, have applied this solution to the growth of multi-phase binary systems.

A general solution for the layer growth of a ternary system was provided by Kirkaldy [150–151]. This solution was applied by Kirkaldy and Brown[8] to the study of the growth of several two-phase Cu–Zn–Sn diffusion couples and was recently used by Nesbitt and Heckel [153] to study several two-phase Ni–Cr–Al diffusion couples. Most recently, Jan et al. [154] applied this solution to the growth of multi-phase ternary diffusion couples. Presentation of the mathematical development for the growth of a multi-phase ternary diffusion couple system as given below follows closely that of Jan et al.[154].

Figure 25 shows the concentration profiles, C_i-x curves, with i being components 1 and 2, respectively, for the growth of a three-phase ternary diffusion couple and the corresponding ternary phase diagram at constant temperature T and pressure p. The three-phase ternary diffusion couple is used to illustrate the principles involved. These results can be generalized readily to the growth of an n-phase system. The nomenclatures used here are given in Table 8. During the growth (or dissolution) of the three phases, α, β, and γ, mass balances must be maintained at all the interfaces, α/β and β/γ, in addition to the overall mass

balance of the couple. Since only two of the three component concentrations are independent, the following two interface mass balance equations for each of the two interfaces apply. For the α/β interface,

$$\left(c_i^{\alpha,\beta} - c_i^{\beta\alpha}\right)\frac{d\zeta^{\alpha,\beta}}{dt} = \tilde{J}_i^{\alpha,\beta} - \tilde{J}_i^{\beta\alpha} \qquad (5a,b)$$

with i = 1,2. The diffusive flux terms $\tilde{J}_i$ are related to the four interdiffusion coefficients, $\tilde{D}_{11}$, $\tilde{D}_{12}$ (again with i = 1,2) by the following equation:

$$\tilde{J}_i^{\alpha} = -\tilde{D}_{i1}^{\alpha}\frac{\partial C_1}{\partial x} - \tilde{D}_{i2}\frac{\partial C_2}{\partial x} \qquad (6a,b)$$

There are two similar relations for the diffusive fluxes in the β-phase, $\tilde{J}_i^{\beta}$'s. Substituting Equations 6a and 6b into Equations 5a and 5b and rearranging the terms yields

$$\frac{d\zeta^{\alpha,\beta}}{dt} = \frac{\left[\left(-\tilde{D}_{i1}^{\alpha}\frac{\partial C_1}{\partial x}\right)^{\alpha,\beta} + \left(-\tilde{D}_{i2}^{\alpha}\frac{\partial C_2}{\partial x}\right)^{\alpha,\beta}\right] - \left[\left(-\tilde{D}_{i,1}^{\beta}\frac{\partial C_1}{\partial x}\right)^{\alpha,\beta} + \left(-\tilde{D}_{i2}^{\beta}\frac{\partial C_2}{\partial x}\right)^{\alpha,\beta}\right]}{\left[C_i^{\alpha,\beta} - C_i^{\beta\alpha}\right]}\frac{1}{\sqrt{t}}$$

$$= \frac{\left[-\tilde{D}_{i1}^{\alpha}K_1^{\alpha,\beta} - \tilde{D}_{i2}^{\alpha}K_2^{\alpha,\beta} + \tilde{D}_{i1}^{\beta}K_1^{\beta\alpha} + \tilde{D}_{i2}^{\beta}K_2^{\beta\alpha}\right]}{\left[C_i^{\alpha,\beta} - C_i^{\beta\alpha}\right]}\frac{1}{\sqrt{t}} \qquad (7a,b)$$

where

$$K_i^{\alpha,\beta} = \left(\frac{dC_i}{d\lambda}\right)^{\alpha,\beta} = \sqrt{t}\left(\frac{\partial C_i}{\partial x}\right)^{\alpha,\beta} \qquad (8a)$$

$$K_i^{\beta\alpha} = \left(\frac{dC_i}{d\lambda}\right)^{\beta\alpha} = \sqrt{t}\left(\frac{\partial C_i}{\partial x}\right)^{\beta\alpha} \qquad (8b)$$

Values of $K_i^{\alpha,\beta}$ and $K_i^{\beta\alpha}$ are complex functions of $\tilde{D}_{i1}^{\alpha}$, $\tilde{D}_{i2}^{\alpha}$, $\tilde{D}_{i1}^{\beta}$, $\tilde{D}_{i2}^{\beta}$, $C_i^{\alpha,\beta}$ and $C_i^{\beta\alpha}$ as given in detail elsewhere [154]. Values of $C_i^{\alpha,\beta}$ and $C_i^{\beta,\alpha}$ are obtained from the solution of the Fick's second law. By assuming constant $\tilde{D}_{i1}$'s and $\tilde{D}_{i2}$'s and integrating Equations 7a and 7b, the following equations may be obtained:

$$\zeta^{\alpha,\beta} = \frac{2\left[-\tilde{D}_{i1}^{\alpha}K_1^{\alpha,\beta} - \tilde{D}_{i2}^{\alpha}K_2^{\alpha,\beta} + \tilde{D}_{i1}^{\beta}K_1^{\beta\alpha} + \tilde{D}_{i2}^{\beta}K_2^{\beta\alpha}\right]\sqrt{t}}{\left[C_i^{\alpha,\beta} - C_i^{\beta\alpha}\right]} \qquad (9a,b)$$

$$= Z^{\alpha,\beta}\sqrt{t}$$

Equations similar to Equations 9a and 9b for $\xi^{\beta,\gamma}$ can be obtained. The width of the β-phase layer as a function of time is

$$w^{\beta} = \xi^{\beta\gamma} - \xi^{\alpha,\beta} = 2\left\{\frac{\left[-\tilde{D}_{i1}^{\beta} K_1^{\beta\gamma} - \tilde{D}_{i2}^{\beta} K_2^{\beta\gamma} + \tilde{D}_{i1}^{\gamma} K_1^{\gamma,\beta} + \tilde{D}_{i2}^{\gamma} K_2^{\gamma,\beta}\right]}{\left[C_i^{\beta\gamma} - C_i^{\gamma,\beta}\right]} - \frac{\left[-\tilde{D}_{i1}^{\alpha} K_1^{\alpha,\beta} - \tilde{D}_{i2}^{\alpha} K_2^{\alpha,\beta} + \tilde{D}_{i1}^{\beta} K_1^{\beta\alpha} + \tilde{D}_{i2}^{\beta} K_2^{\beta\alpha}\right]}{\left(C_i^{\alpha,\beta} - C_i^{\beta\alpha}\right)}\right\}\sqrt{t}$$

$$= \left[Z^{\beta\gamma} - Z^{\alpha,\beta}\right]\sqrt{t} = W^{\beta}\sqrt{t} \qquad (10a,b)$$

If the interdiffusion coefficients for all three phases, α, β and γ are known, the above equations may be used to calculate the growth of β as a function of time at constant temperature. The above equation can be generalized for the growth of an arbitrary phase in a multi-phase ternary system [154].

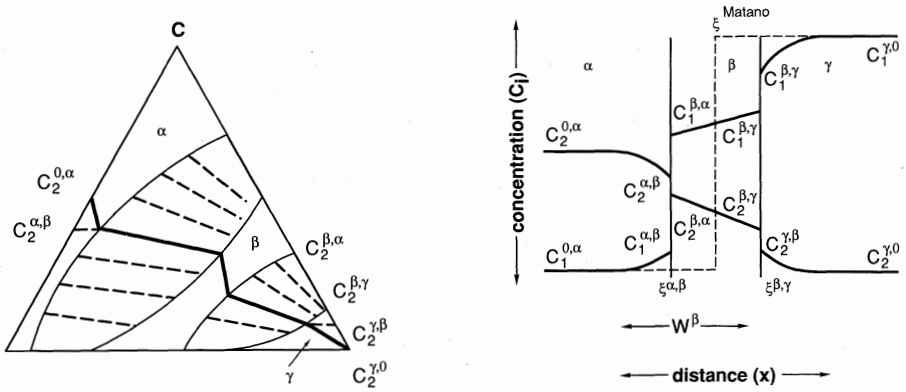

Figure 25 The relationship between the diffusion zone interface concentrations of a three-phase ternary diffusion couple at constant temperature and pressure, and the isothermal phase diagram for this ternary system.

Table 8. Thermodynamic and Kinetic Nomenclatures

C_1, C_2, C_3	Concentrations of components 1, 2, 3; $C_1 + C_2 + C_3 = 1$.
C_i	Concentrations of component i with i = 1 or 2.

D_1, D_2, D_3	Intrinsic diffusion coefficients of a ternary phase, neglecting the cross-intrinsic diffusion coefficients.
$\tilde{D}_{11}, \tilde{D}_{12}, \tilde{D}_{21}, \tilde{D}_{22}$	Interdiffusion coefficients of a ternary phase.
$\tilde{D}_{i1}, \tilde{D}_{i2}$	Interdiffusion coefficient of a ternary phase with i = 1 or 2.
$\tilde{J}_1, \tilde{J}_2, \tilde{J}_3$	Diffusive fluxes of components 1, 2, 3.
$\tilde{J}_i$	Diffusive flux of component i with i = 1 or 2.
$\tilde{J}_i^{\beta,\alpha}$	The superscript β, α refers to the flux of component i in the β-phase at the α/β interface.
$\tilde{K}_i^{\alpha,\beta}$	$\left[\frac{dC_i}{d\lambda}\right]^{\alpha,\beta} = \sqrt{t}\left[\frac{\partial C_i}{\partial x}\right]^{\alpha,\beta}$ with i = 1 or 2
$\tilde{K}_i^{\beta,\alpha}$	$\left[\frac{dC_i}{d\lambda}\right]^{\beta,\alpha} = \sqrt{t}\left[\frac{\partial C_i}{\partial x}\right]^{\beta,\alpha}$ with i = 1 or 2
P	Pressure.
t	Time.
T	Absolute temperature in K, °C = K - 273.
w^β	Thickness of a β-phase growing from a α/ϒ couple = $\xi^{\beta,\Upsilon}-\xi^{\alpha,\beta}$.
W^β	A parameter relating w^β and $\sqrt{t} = [z^{\beta,\Upsilon}-z^{\alpha,\beta}]$.
x	Distance coordinate.
$\xi^{\alpha,\beta}$	Position of the α/β interface = $z^{\alpha,\beta}\sqrt{t}$.
$\xi^{\beta,\Upsilon}$	Position of the β/ϒ interface = $z^{\beta,\Upsilon}$ and $\sqrt{t}$
$Z^{\alpha,\beta}$	A parameter relating $\xi^{\alpha,\beta}$ and $\sqrt{t}$ $= \dfrac{2[-\tilde{D}_{i1}^{\alpha}K_1^{\alpha,\beta} - \tilde{D}_{i2}^{\alpha}K_2^{\alpha,\beta} + \tilde{D}_{i1}^{\beta}K_1^{\beta,\alpha} + \tilde{D}_{i2}^{\beta}K_2^{\beta,\alpha}]}{[C_i^{\alpha,\beta} - C_i^{\beta,\alpha}]}$
$Z^{\beta,\Upsilon}$	A parameter relating $\xi^{\beta,\Upsilon}$ and $\sqrt{t}$

$$= \frac{2[-\tilde{D}_{i1}^{\beta} K_1^{\beta,\gamma} - \tilde{D}_{i2}^{\beta} K_2^{\beta,\gamma} + \tilde{D}_{i1}^{\gamma} K_1^{\gamma,\beta} + \tilde{D}_{i2}^{\gamma} K_2^{\gamma,\beta}]}{[C_i^{\beta,\gamma} - C_i^{\gamma,\beta}]}$$

Unfortunately, for systems of technological interests not only in soldering, but also in other materials fields such as metallization of compound semiconductors, quantum-well layered structures and structural composites, these data are not known. Jan et al. [154] had proposed a methodology to obtain the needed values from an analysis of the layer growth as a function of time and the concentration profiles across the diffusion couples. They applied this methodology to obtain interdiffusion and intrinsic diffusion coefficients of T–Ni_3GaAs from the GaAs/Ni couples [154, 155] and interdiffusion coefficients of NbAs and $NbGa_3$ from GaAs/Nb couples [156]. This type of approach should be applied to diffusion couples of soldering systems to provide engineering data for processing improvements and soldering reliability. At the same time, this type of study will provide a basic understanding of the thermodynamic, kinetic and morphological stabilities at materials interfaces.

NUMERICAL MODELS FOR GROWTH

In previous sections, the thermodynamic and kinetic equations that describe the volume diffusion controlled intermetallic growth process were developed. Under ideal conditions, the differential equations (diffusion equations) that describe the growth process can be solved analytically in closed form. However, under many real conditions analytical solutions do not exist and numerical solutions are required. Several common situations where analytical solutions do not exist include cases where the initial concentration profile is complex (not constant or described by a simple error function), where boundary compositions are not constant and vary as impingement occurs, where the diffusion coefficient is compositionally dependent and where diffusion occurs under non-isothermal conditions. There are a variety of numerical methods that can be used to solve this class of problems. The most important numerical methods are the finite difference method, the Crank-Nicolson method, the method of lines and the method of finite elements. Each numerical approach has advantages and disadvantages relative to the others. If numerical techniques are used, it is very important that a problem very similar to the one under consideration be contrived that can be solved analytically and numerically (such as if the actual problem involves non-isothermal diffusion, solve it isothermally first by using both methods). A comparison of results will insure the validity of the approach before the actual problem is solved. For further details, refer to a recent review article by Romig, et. al. [157], describe the merits and limitations of each numerical approach and also lists useable computer codes.

In cases where growth is controlled by interfacial reactions, the growth process can be modeled without solving the differential equation that describes volume diffusion. The interfacial controlled reaction will be described by a linear equation in time. To model growth, reaction is simply numerically integrated over the given time dependent thermal cycle.

EXAMPLE OF MICROSTRUCTURAL EVOLUTION MODELING OF RELIABILITY

Intermetallic Layer Growth Between Au Thick Films and Pb–In Solder

In this example, the intermetallic growth kinetics between 50Pb–50In solder and two Au thick films are described. The growth kinetics in each were analyzed and quantitative reaction rates determined. These results were used to analyze the long-term microstructural evolution of the solder joints under severe thermal conditions (such as under the hood of an automobile). In this case, the Pb is not chemically involved and the diffusional process is really based on a simple binary reaction between Au and In. Furthermore, only one intermetallic compound is formed and the simple layer growth analysis is fully valid. It is important to understand immediately that this reliability analysis only addresses microstructural evolution in the joint and does not address how that evolution might influence the properties and behavior of that joint.

The design engineer had two choices for the thick-film alloy: a nominally pure Au film (Au plus glasses and organics that form thick-film ink) and a Au– 3 wt.% Pd film (same ration of total metal to non-metals in the ink). The pure Au has lower electrical resistance and is very solderable. The Au–Pd ink has a slightly higher resistance and is less solderable, but it was known qualitatively to react more slowly with the Pb–In solder than the pure Au ink. To choose between the two, it was necessary to determine the reaction rates quantitatively and use those results to model microstructural evolution under the service environment.

Figure 26A shows the time dependence of layer growth for the pure Au alloy. The reaction rates are linear in time indicative of a reaction controlled by interfacial kinetics. Figure 26B shows the time dependence of layer growth for the Au–Pd thick-film alloy. In both cases, the intermetallic layer formed is pure $AuIn_2$. The Pb is excluded as small islands in the microstructure. As qualitative comparison does confirm that the Au–Pd metallization reacts more slowly with the Pb–In solder in the solid state than the pure Au metallization. A classical Arrhenius rate analysis can be performed on these data, as shown in Figure 9. The Arrhenius analysis correlates the growth rates (slopes: thickness/time) to reciprocal absolute temperature. As can be seen in Figure 9, the Au–Pd thick-film metallization reacts more slowly than the pure Au metallization. For a complete description of the kinetic study, the reader is referred to the literature [158].

Given the thermal environment the solder joint must function in, it is a simple matter to integrate the kinetics through the given thermal profile. Figure 27 shows the results of the microstructural evolution reliability calculation. The *life* of the joint here is defined as the point at which the Au thick films are completely reacted, leaving the intermetallic compound layer in intimate contact with the

ceramic substrate. Under the given thermal environment, it can be shown that the life of the Au–Pd film will be approximately five times greater than that of the pure Au film. This margin was still inadequate, so a decision was made to double the thickness of the thick-film metallization, giving the order of magnitude life increase shown in Figure 27. Again, the reader is warned that this life prediction is based *only* on microstructural evolution and does **not** consider the mechanical properties and behavior of the joint after the Au thick film has been fully consumed and converted to intermetallic compound.

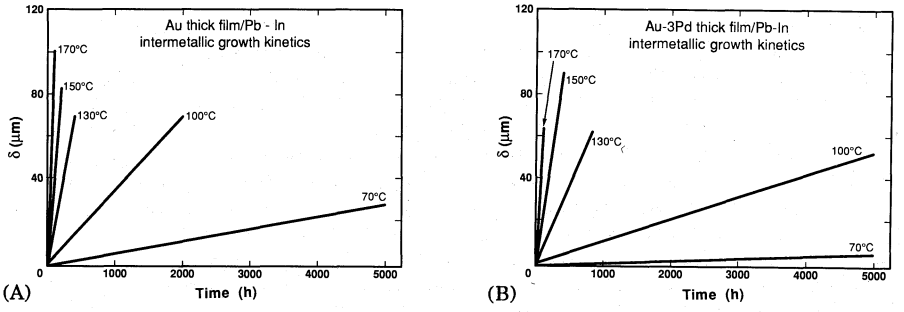

Figure 26 Growth kinetics of $AuIn_2$ between Pb–In solder and (A) pure Au,and (B) Au–Pd, thick films. Linear kinetics indicative of interfacial control.

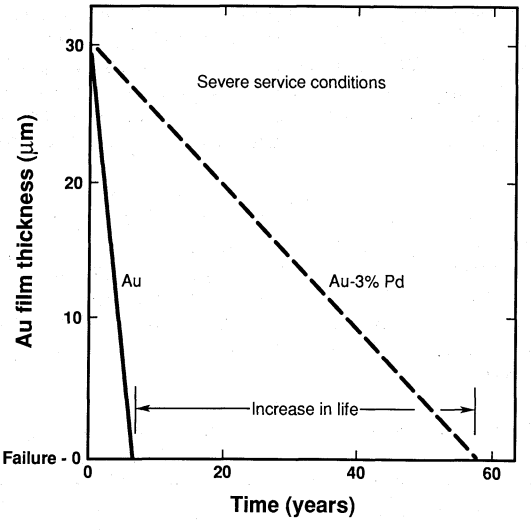

Figure 27 Microstructural evolution prediction of joint lifetime for Au and Au–Pd thick-film metallizations in contact with Pb–In solder.

Future Concerns

This chapter has shown that there is a significant level of understanding, both fundamental and empirical, of the reactions that occur at solder–substrate

interfaces. Wetting behavior, intermetallic phase formation and intermetallic growth rates can be predicted and modeled empirically or, in some cases, from fundamental principles. However, the understanding of solder–substrate reactions is not yet complete and is an area in which additional research is needed. The following is a summary of areas where the state of knowledge is incomplete and areas in which there is likely to be future activity.

WETTING

The mechanisms that control the wettability of a metal or metallization by liquid solder using a mild electronics grade flux are, in general, understood. Knowledge is incomplete on a variety of apparently second-order effects that can significantly influence wetting behavior. Very low levels of impurities in the solder, or contamination of the solder by leached metallization, can have marked effects on the growth rates of oxide films or of intermetallic compounds. Very low levels of impurities in storage, particularly H_2S, SO_2, HCl, and carboxylic acids that are emitted from anisotropic coatings and packaging materials, can have a significant effect on wettability. Furthermore, the effect of intermetallic formation on solderability, especially with regard to the wetting behavior of intermetallic layers, is not known. As discussed previously, the presence of some intermetallics (such as Cu_6Sn_5) inhibits wetting while others have a negligible effect on wetting. This apparently inconsistent behavior must be explored in more detail.

The wetting balance is becoming the standard technique for quantitative measurements of wettability. It is a flexible instrument that can be configured with either a solder bath or a solder globule into which the component is dipped. Considerable work is in progress to develop standard procedures for the use of the wetting balance. Standardized methods are required to obtain traceable measurements and allow for data comparison and exchange within the soldering community.

The true relationship between solderability and wettability has yet to be determined. While one can now measure wettability in a quantitative way, good wettability does not ensure good solderability. Thermal profiles and actual joint geometry obviously are part of the relationship, but their quantitative role has not been described. Clearly, one desperate need is to relate, explicitly, wettability of a substrate, for a given solder and flux at a given temperature, to the solderability of the actual component.

It is universally accepted that component solderability is intimately linked with product reliability, but only recently have quantitative links begun to be established. There are two aspects. First, poor solderability leads to poor first-pass soldering yields and therefore significant amounts of rework. Secondly, poor component solderability leads to a wide range of solder fillet geometries on a particular component type. This variability in solder fillet geometry leads to a wide variation in solder joint impact and fatigue strengths. Research has recently begun to correlate, in a quantified manner, component solderability as measured with a wetting balance to solder fillet geometry and in turn fatigue lifetime.

Electronic components are sold for a price based on their electronic performance, not on their solderability. An electronics assembly typically will not be scrapped if it is not solderable. However, a stronger flux will need to be used or the amount of rework will be increased, neither of which is really acceptable. It is imperative that all problems of component solderability be reported to the component manufacturer. The manufacturer often knows how to produce components with good solderability, but often will not to contain costs. This is clearly a case where it is more cost effective to purchase parts with good solderability rather than only on the basis of lowest cost.

INTERMETALLIC PHASE FORMATION

As mentioned previously, there are quantitative models available to predict phase formation in an n-component system. Of particular utility is the combined computational-experimental approach. The information needed for this model to be used effectively is the experimental data (phase diagrams) of n-component solder–substrate systems of interest. A number of experiments in this area are being performed and it is expected that this effort will continue and grow. These types of analyses are essential if reliable solder–substrate microstructural evolution models are to be developed.

INTERMETALLIC GROWTH

The area of intermetallic growth has been extensively studied and a number of empirical relationships developed. However, the data is widely varied and often conflicting. Furthermore, it is extremely dangerous to extrapolate empirical kinetic relationships beyond the temperature range over which they were measured.

In order to improve upon this state of understanding of intermetallic growth, precise experimentation and analysis is needed. Fundamental data is required so that phenomenological (thermokinetic) models can be developed. With fundamental mechanistic models, one can extrapolate with far greater certainty than is possible with empirical models.

EFFECT OF INTERMETALLICS ON SOLDER JOINT PROPERTIES

The presence of intermetallics in a solder joint usually indicates that a good metallurgical joint has formed. However, an important question that remains is what effect intermetallics have on the mechanical integrity of a solder joint. Intermetallics are usually considered to be brittle, but virtually no mechanical property data on the intermetallic compounds that form in solder joints has been measured. Hence, the degree to which the presence of intermetallics in solder joints is deleterious to mechanical integrity is not known. Careful mechanical studies of solder joints with varying compositions and volume percentages of intermetallics are needed. In addition, fundamental mechanical and physical property measurements of the pure intermetallic compounds are also sorely needed. Specifically, the mechanical behavior of a solder joint needs to be correlated to the extent of microstructural evolution in that solder joint.

Acknowledgements

The authors would like to thank Drs. Paul Vianco and Fred Yost for helpful comments and review of the manuscript. The portion of this work performed at

Sandia National Laboratories and supported by the U.S. DOE under Contract Number DE–AC04–76DP00789.

References

1. R. J. Klein-Wassink, *Soldering in Electronics*, 2nd Ed. Electrochemical Publications, Ayr, Scotland, 1989.

2. C. Lea, *A Scientific Guide to Surface Mount Technology,* Electrochemical Publications, Ayr, Scotland, 1989.

3. H. H. Manko, *Solders and Soldering*, McGraw–Hill, New York, New York, 2nd edition, 1979.

4. ITRI – International Tin Research Institute, Middlesex, England. Many papers on solderability issues.

5. P. G. DeGennes, *Reviews in Modern Physics,* 1985, vol. 57, pp. 827.

6. F. J. Yost and A. D. Romig, Jr., "Thermodynamics of Wetting by Liquid Metals," *Electronic Packaging Materials Science*, Materials Research Society, 1988, p 385.

7. R. J. Klein-Wassink, *J. Inst. Metals,* 1967, vol. 95, pp. 38.

8. S. Teed and V. C. Marcotte, *Proc. 11th N. Amer. Thermal Anal. Soc.*, 1981, vol. 2, pp. 77.

9. M. A. Nasta, G. R. Hill and D. Campbell, *Soldering and Surface Mount Tech.*, 1990, vol. 4, pp. 5.

10. L. Pessel, *Proc. 59th Ann. Meeting,* 1956, pp. 159–174, ASTM.

11. J. A. ten Duis and E. van der Muelen, *Philips Tech. Rev.*, 1967, vol. 28, pp. 362.

12. B. M. Allen, *Welding and Metal Fabrication,* Jan/Feb. 1982, pp. 47.

13. D. R. Wallis, *Brazing and Soldering,* 1982, vol. 3, pp..

14. K. M. Lin and T. R. Harry, *The Western Electric,* Spring 1982, pp. 11.

15. D. MacKay, *Circuits Manufacturing,* 1973, vol. 13, pp. 52.

16. G. Becker, *Brazing and Soldering,* 1983, vol. 5, pp. 40.

17. W. Abbot, *119th TMS Annual Meeting*, Anaheim, CA, Feb. 1990.

18. J. G. Davy, *Proc. ASM Microelectronic Packaging and Tech. Conf.*, 1989, pp. 443.

19. D. T. F. Roberts, *Brazing and Soldering,* 1983, vol. 4, pp. 28.

20. J. Haimovich, *Welding Journal,* 1989, vol. 8, no. 3, Research Supplement, 102s.

21. T. B. Massalski, ed., *Binary Alloy Phase Diagrams*, American Society for Metals, Metals Park, OH,1986, vols. 1 and 2.

22. P.-Y. Chevalier, *Thermochimica Acta,* 1988, vol. 130, pp. 1.

23. I. Ansara and J. P. Nabot, *Thermochimica Acta*, 1988, vol. 129, pp. 89.

24. F. G. Yost and A. D. Romig, Jr., *Storage Life of Thermal Detents*, SAND84–0678, 1984, Sandia National Laboratories, Albuquerque, NM.

25. A. D. Romig, Jr., F. G. Yost and P. F. Hlava, *Microbeam Analysis – 1984*, ed. A. D. Romig, Jr. and J. I. Goldstein, San Francisco Press, San Francisco, CA, 1984, pp. .

26. A. Prince, *Journal of the Less Common Metals,* 1967, vol. 12, pp. 107.

27. M. M. Karnowsky and A. Rosenzweig, *Trans. TMS–AIME,* 1968, vol. 242, pp. 2257.

28. G. Humpston and B. L. Davies, *Metal Science,* 1984, vol. 18, pp. 329.

29. G. Humpston and D. S. Evans, *Materials Science and Technology,* 1987, vol. 3, pp. 621.

30. M. M. Karnowsky and F. G. Yost, *Metall. Trans. A,* 1976, vol. 7A , pp. 1149.

31. D. S. Evans and A. Prince, *Metal Science,* 1977, vol. 11, p. 597.

32. V. C. Marcotte and M. W. Ricker, *Metall. Trans. A,* 1981, vol. 12A, pp. 2136.

33. V. K. Nikitina and Y. K. Lobanova, *Inorganic Materials* (trans. volume of *Izvestiya Akademii Nauk SSSR, Neorganicheskie Materialy*), 1974, pp. 1376.

34. W. Hofmann, *Lead and Lead Alloys – Properties and Technology*, Springer–Verlag, 1970, pp. 149.

35. Y. A. Chang, ed., *The Metallurgy of Copper Phase Diagrams and Thermodynamic Properties of Ternary Cu–Metal Systems,* 1979, INCRA Monograph, vol. 6, pp. 631.

36. V. C. Marcotte and K. Schroder, *Materials Research Society Symposium Proceedings,* 1983, vol.19, pp. 403.

37. M. V. Pikunov, V. A. Volkov, and N. E. Verbov, *Izv. Vyssh. Uchebn. Zaved., Tsvetn. Metall.,* 1983, vol. 5, pp. 128.

38. I. Okamoto and T. Yasuda, *Trans. JWRI*, 1986, vol. 15, no. 2, pp. 73.

39. M. K. Bhargava and K. Schubert, *Z. Metallkunde,* 1976, vol. 67, pp. 318.

40. V. N. Eremenko, L. E. Pechentkovskaya, and M. M. Churakov, *Fiz. Khim. Obrab. Mater.,* 1976, vol. 3, p. 124.

41. V. H. Eremenko, M. M. Churakov, and L. E. Pechentkovskaya, *Russian Metallurgy,* 1976, vol. 4, pp. 53.

42. Z. P. Saperstein and M. A.Howes, *Welding Journal,* 1968, vol. 47, no. 4, pp. 162s, Research Supplement.

43. M. A.Howes and Z. P. Saperstein, *Welding Journal,* 1969, vol. 48, no.2, pp. 80, Research Supplement.

44. W. G. Bader, *Welding Journal,* 1969, vol. 48, no. 12, pp. 551s, Research Supplement.

45. H. Berg and E. L. Hall, *11th Annual Proceedings: Reliability Physics,* 1973, pp. 10.

46. J. Romer, *Schweisstechnik,* 1974, vol. 24, no. 3, pp. 100.

47. W. G. Bader, *Welding Journal,* 1975, vol. 54, no. 10, pp. 370s, Research Supplement.

48. H. Heinzel and K. E. Saeger, *Gold Bulletin,* 1976, vol. 9, pp. 7.

49. F. G. Yost, *Gold Bulletin,* 1977, vol. 10, pp. 94.

50. P. W. DeHaven, G. A. Walker and N.A. O'Neil, *Advances in X–ray Analysis,* vol. 27, Plenum Publishing Corp., 1984, pp. 389.

51. V. C. Marcotte, A Study of Liquid Solder (80Au–20Sn)–Copper Reactions During Thermal Cycling, Presented at *ASM Materials Week*, Cincinnati, OH, October, 1987.

52. M. M. Karnowsky, *The Gold–Tin–Lead Alloys, Part I: Physical and Electrical Properties of Selected Compositions*,, SC–DC–67–1733, 1967, Sandia Laboratories, Albuquerque, NM.

53. M. H. Bester, *Proceedings of the International Electronic Packaging and Production Conference*, Brighton, England, Oct. 1968, pp. 211.

54. W. G. Bader, *Physical Metallurgy of Metal Joining*, R. Kossowsky and M. E. Glicksman, eds.,1981, p. 260, The Metallurgical Society of A.I.M.E.

55. J. M. Lommel and B. Chalmers, *Trans. TMS–AIME*, 1959, vol. 215, p. 499.

56. D. R. Frear, D. Grivas, and J. W. Morris, Jr., *J. Electron. Mats.*, 1987, vol. 16, pp.18.

57. B. L. Janco and J. D. Braun, *Metallographic Review*, 1973, vol. 2, pp.16 .

58. J. D. Braun, *ASM Transactions Quarterly*, 1963, vol. 56, no. 4, pp. 870.

59. A. D. Romig, Jr., unpublished research, Sandia National Laboratories, 1986; see also J. J. Stephens and A. D. Romig, Jr., Compatibility of Au Base Thick Films With Solder Alloys, *Proceedings of the 16th DOE Compatibility Conference*, Lawrence Livermore National Laboratory, Livermore, CA, April, 1990.

60. P. J. Kay and C. A. MacKay, *Transaction of the Institute of Metal Finishing,* 1973, vol. 51, pp. 85.

61. J. J. Stephens, internal memorandum, March 2, 1989, Sandia National Laboratories, Albuquerque, NM.

62. J. D. Braun and T. B. Rhinehammer, *ASM Transactions Quarterly*, 1963, vol. 56, no. 4, pp. 870.

63. M. M. Robertson and M. M. Karnowsky, *Gold–Tin and Gold–Tin–Lead Diffusion Couples,* SC–TM–68–728, December, 1968, Sandia National Laboratories, Albuquerque, NM.

64. R. E. Sulouff, *International Microelectronics Symposium–1974*, Boston, MA, pp. 41, International Society for Hybrid Microelectronics.

65. F. G. Yost, F. P. Ganyard, and M. M. Karnowsky, *Metall. Trans. A*, 1976, vol. 7A, pp. 1141.

66. S. J. Muckett, M. E. Warwick, and P. E. Davis, *Plating and Surface Finishing,* 1986, vol. 73, no. 1, pp 44.

67. J. J. Stephens, H. S. Scully, and A. D. Romig, unpublished research, Sandia National Laboratories, 1990.

68. L. Zakraysek, *Welding Journal*, 1972, vol. 51, no. 11, pp. 536s, Research Supplement.

69. M. Onishi and H. Fujibuchi, *Transactions of the Japanese Institute of Metals*, 1975, vol. 16, pp. 539.

70. D. A. Unsworth and C. A. MacKay, *Transactions of the Institute of Metal Finishing*, 1973, vol. 51, p. 85.

71. K. Kumar, A. Moscaritolo, and M. Brownawell, *Journal of the Electrochemical Society*, 1981, vol. 128, pp. 2165.

72. J. C. Fister and J. F. Breedis, *Copper Alloys For Avoidance of Interdiffusion in Electronic Packages*, Presentation to the IEPS Conference, Itasia, IL, October 25, 1983.

73. V. C. Marcotte and K. Schroder, *Materials Research Society Symposium Proceedings*, 1983, vol. 19, pp. 403.

74. D. S. Dunn, T. F. Marinis, W. M. Sherry, and C. J. Williams, *Electronic Packaging Materials Science,* E. A. Geiss, K. N. Tu, and D. R. Uhlman, eds., 1985. pp. 129, Materials Research Society.

75. B. G. LeFevre and R. A. Barczykowski, *Wire Journal International*, January, 1985, pp. 65.

76. E. K. Ohriner, *Welding Journal,* 1987, vol. 66, no. 7, pp. 191s, Research Supplement.

77. Q. Yiyu, F. Hongyuan, C. Dinghua, F. Fuhua, and H. Lixia, *Brazing and Soldering*, Autumn, 1987, vol. 13, pp. 39.

78. P. J. Kay and C. A. MacKay, *Transactions of the Institute of Metal Finishing,* 1979, vol. 57, pp. 169.

79. V. C. Marcotte and N. G. Koopman, *IEEE Transactions on Components, Hybrids and Manufacturing Technology,* 1982, CHMT–5, no. 4, pp. 395.

80. M. E. Warwick and S. J. Muckett, *Circuit World*, 1983, vol. 9, no. 4, pp. 5.

81. H. N. Keller, *IEEE Transactions on Components, Hybrids, and Manufacturing Technology*, 1986, CHMT–9, no. 4, pp. 433.

82. D. R. Frear, *Intermetallic Aging Studies of Soldered Paliney 7*, Internal Memorandum, November 11, 1989, Sandia National Laboratories, Albuquerque, NM.

83. *ASM Metals Handbook*, Metallography and Microstructures, 9th Ed., 1985, vol. 9, ASM International.

84. J. I. Goldstein, D. E. Newbury, P. Echlin, D. C. Joy, C. Fiori, and E. Lifshin, *Scanning Electron Microscopy and X–Ray Microanalysis*, Plenum Press, NY, 1981.

85. D. R. Frear, J. B. Posthill, and J. W. Morris, Jr., *Metall. Trans. A*, 1989, vol. 20A, p. 325.

86. D. C. Joy, A. D. Romig, Jr., and J. I. Goldstein, *Principles of Analytical Electron Microscopy,* Plenum Press, NY, 1986.

87. W. Edington, *Practical Electron Microscopy in Materials Science*, Philips Electronic Instruments Electron Optics Publishing Group, Mahwah, NJ, 1976.

88. L. Revay, Interdiffusion and Formation of Intermetallic Compounds in Tin–Copper Alloy Surface Coatings, *Surface Technology*, 1977, vol. 5, pp. 57.

89. B. D. Dunn, *Metallurgical Assessment of Spacecraft Parts and Materials*, Chichester, England: Ellis Horwood Ltd. (Distributed in US by Simon & Schuster), 1989. pp. 278.

90. R. J. Klein-Wassink, *Soldering in Electronics*, 2nd ed., Ayr, Scotland, Electrochemical Publications, Ltd, 1989, p. 156.

91. K.-C. Hsieh and Y. A. Chang, *Can. Met. Q.*, 1987, vol. 26, p. 311.

92. J.-C. Lin, PhD Thesis, University of Wisconsin, Madison, WI, 1986.

93. Y.-Y. Chuang, PhD Thesis, University of Wisconsin, Madison, WI, 1983.

94. T.-W. L. Ngai, PhD Thesis, University of Wisconsin, Madison, WI, 1987.

95. A. Bolcavage, Y. A. Chang and A. D. Romig, Jr., ongoing research, 1990.

96. W. J. Boettinger and U. Kattner, NIST, Gaithersburg, MD, 1990, private communication.

97. K.-C. Chou and Y. A. Chang, *Ber. Bunsenges. Phys. Chem.*, 1989, vol. 93, p. 735.

98. A. D. Romig, Jr., *Bulletin of Alloy Phase Diagrams*, 1986, vol. 8, p. 308.

99. L. S. Darken, *Trans. TMS–AIME*, 1942, vol. 150, p. 157.

100. J. S. Kirkaldy, *Can. J. Phys.*, 1958, vol. 36, p. 917.

101. W. Jost, *Diffusion in Liquids, Solids and Gases*, Academic Press, NY, 1960.

102. J. I. Goldstein and R. E. Ogilvie, *X–Ray Optics and Microanalysis*, Herman Press, Paris, 1966, p. 594.

103. A. D. Romig, Jr. and J. I. Goldstein, Applications of Phase Diagrams in Metallurgy and Ceramics, NBS Special Publication SP–496, 1977, p. 462.

104. J. W. Gibbs, *The Collected Works of J. W. Gibbs*, 1957, vol. 1, Yale University Press, New Haven, p. 55.

105. M. Hillert, *Jerkorntorets Ann.*, 1957, vol. 141, p. 757.

106. J. C. Brice, *J. Crystal Growth*, 1967, vol. 1, p. 218.

107. H. B. Aaron and G. R. Kotler, *Metall. Trans.*, 1971, vol. 2, p. 393.

108. J. S. Langer and R. F. Sekerka, *Acta Metall.*, 1975, vol. 23, p. 1225.

109. J. W. Cahn and F. Larche, *Acta Metall.*, 1982, vol. 30, p. 51.

110. W. C. Johnson and J. I. D. Alexander, *J. Appl. Phys.*, 1986, vol. 59, no. 8, p. 2735.

111. P. W. Voorhees and W. C. Johnson, *J. Chem. Phys.*, 1986, vol. 84, no. 9, p. 5108.

112. A. D. Romig, Jr. and J. I. Goldstein, *Metall. Trans. A*, 1983, vol. 14A, p. 1224.

113. D. R. Gaskell, *Introduction to Metallurgical Thermodynamics*, McGraw Hill, NY, 1981.

114. J. I. Goldstein and R. E. Ogilvie, *Trans. TMS–AIME*, 1965, vol. 233, p. 2083.

115. A. S. Doan and J. I. Goldstein, *Metall. Trans.*, 1970, vol. 1, p. 1759.

116. A. D. Romig, Jr. and J. I. Goldstein, *Metall. Trans. A*, 1980, vol. 11A, p. 1151.

117. A. D. Romig, Jr. and J. I. Goldstein, *Metall. Trans. A*, 1981, vol. 12A, p. 243.

118. D. C. Dean and J. I. Goldstein, *Metall. Trans.A*, 1986, vol. 17A, p. 1131.

119. A. D. Romig, Jr. and J. C. Mabon, *J. Phase Equilibria*, 1991, to be submitted.

120. J. S. Kirkaldy and L. C. Brown, *Can. Met. Q.*, 1963, vol. 2, p. 89.

121. F. J. J. Van Loo, J. A. Van Beck, and G. F. Bastin, *Solid State Ionics*, 1985, vol. 16, p. 131.

122. J. A. Van Beck, P. M. T. Kok, and F. J. J. Van Loo, *Oxid. Met.*, 1984, vol. 22, p. 147.

123. P. Voisters, M. Laheiji, F. J. J. Van Loo, and R. Metselaar, *Oxid. Met.*, 1983, vol. 20, p. 147.

124. F. J. J. Van Loo, J. A. Van Beck, G. P. Bastin and R. Metselaar, *Oxid. Met.*, 1984, vol. 22, p. 161.

125. M. Leute, *Solid State Ionics,* 1985, vol. 17, p. 185.

126. J.-C. Lin, K.-C. Hsieh, K. J. Schulz and Y. A. Chang, *J. Mater. Res.*, 1988, vol. 3, p. 148.

127. J.-C. Lin, X.-Y. Zheng, K.-C. Hsieh, and Y. A. Chang, Epitaxy of Semiconductor Layered Structures, R. T. Tung, L. R. Dawson and R. L. Gunshor, eds., *Mats. Res. Soc. Symp. Proc.*, 1988, vol. 102, p. 233.

128. K. J. Schulz, X.-Y. Zheng, and Y. A. Chang, Electronic Packaging Materials Science III, R. Jaccodine, K. A. Jackson, and R. C. Sundahl, eds., *Mats. Res. Soc. Symp. Proc.*, 1988, vol. 108, p. 455.

129. F.-Y. Shiau, Y. Zuo, X.-Y. Zheng, J.-C. Lin, and Y. A. Chang, Adhesive in Solids, J. E. E. Baglin, D. M. Mattox, C. Batich and R. J. Gottschall, eds., *Mats. Res. Soc. Symp. Proc.*, 1988, vol. 117, p. 171.

130. K. J. Schulz, X.-Y. Zheng and Y. A. Chang, *J. Mater. Res.,* 1989, vol. 4, p. 1462.

131. K. J. Schulz and Y. A. Chang, Advances in Materials, Processing and Devices in III-V Compound Semiconductors, D. K. Sadana, L. Eastman and R. Dupuis, eds., *Mats. Res. Soc. Symp. Proc.*, 1989, vol. 144, p. 557.

132. K. J. Schulz, O. A. Musbah and Y. A. Chang, *J. Appl. Phys.,* 1990, vol. 67, p. 6789.

133. K. J. Schulz, X.-Y. Zheng, J.-C. Lin and Y. A. Chang, *J. Electronic Mater.*, 1990, vol. 19, p. 581.

134. K. J. Schulz, PhD Thesis, University of Wisconsin, Madison, WI, 1988.

135. C. Wagner, *Z. Anorg. Allgem. Chem.*, 1938, vol. 236, p. 320.

136. C. Wagner, *J. Electrochem. Soc.*, 1956, vol. 103, p. 571.

137. M.-X. Zhang, PhD Thesis, University of Wisconsin, Madison, WI, 1990.

138. J.-C. Lin, K. J. Schulz, K.-C. Hsieh, and Y. A. Chang, *J. Electrochem. Soc.*, 1989, vol. 136, p. 3006; also in *High-Temperature Materials Chemistry–IV,* Z. A. Munir, D. Cubicciotti and H. Tagawa, eds., 1988, p. 476, the Electrochem. Soc., Inc. Pennington, NJ.

139. J.-C. Lin and Y. A. Chang, Chemistry and Defects in Semiconductor Heterostructures, M. Kawabe, T. D. Sands, E. R. Weber and R. S. Williams, eds., *Mat. Res. Soc. Symp. Proc.*, 1989, vol. 148, p. 3.

140. Y. A. Chang, *Symposium on High Temperature and Material Chemistry*, Berkeley, CA, 1989, LBL–27905, p. 377.

141. R. M. Rapp, A. Ezis and G. J. Yurek, *Metall. Trans.*, 1973, vol. 4, p. 1283.

142. G. Y. Yurek, R. A. Rapp and J. P. Hirth, *Metall. Trans.*, 1973, vol. 4, p. 1293.

143. S. R. Shatynski, J. P. Hirth, and R. A. Rapp, *Metall. Trans.*, 1979, vol. 10A, p. 591.

144. W. Jost, *Diffusion in Solids, Liquids, and Gases*, 2nd ed., Academic Press, New York, 1960, p. 68.

145. L. S. Castleman, *Nucl. Sci. Eng.*, 1958, vol. 4, p. 209.

146. J. S. Kirkaldy, *Can. J. Phys.*, 1958, vol. 36, p. 917.

147. G. V. Kidson, *J. Nucl. Mater.*, 1961, vol. 3, p. 21.

148. A.-J. Hickl and R. W. Heckel, *Metall. Trans.*, 1975, vol. 6A, p. 431.

149. E. Metin, O. T. Inal, and A. D. Romig, Jr., *Microbeam Analysis – 1988,* ed. D. E. Newbury, San Francisco Press, San Francisco, CA, 1988, pp. 498.

150. J. S. Kirkaldy, *Can. J. Phys.*, 1958, vol. 36, p. 917.

151. J. S. Kirkaldy, *Can. J. Phys.*, 1958, vol. 36, p. 899.

152. J. S. Kirkaldy, *Can. J. Phys.*, 1958, vol. 36, p. 907.

153. J. A. Nesbitt and R. W. Heckel, *Metall. Trans. A*, 1987, vol. 18A, p. 2087.

154. C.-H. Jan, D. Swenson, X.-Y. Zheng, J.-C. Lin, and Y. A. Chang, *Acta Metall.*, 1990, vol. 38, p. 2373.

155. C.-H. Jan, D. Swenson and Y. A. Chang, Fundamentals and Applications of Ternary Diffusion, G. R. Purdy, ed., 1990, p. 127.

156. C.-H. Jan, University of Wisconsin, Madison, WI, 1989, unpublished research.

157. A. D. Romig, Jr., N. Y. Pehlivanturk, and O. T. Inal, *Diffusion Analysis and Applications*, A. D. Romig, Jr. and M. A. Dayananda, eds., 1989, p.45, TMS.

158. A. D. Romig, Jr. and J. J. Stephens, *Metall. Trans. A*, 1991, to be submitted.